Determination of the copper isotope composition of seawater revisited: A case study from the Mediterranean Sea

Isabelle Baconnais, Olivier J. Rouxel, Gabriel Dulaquais, Marie Boye

HAL Id: hal-02345288

https://hal.science/hal-02345288

Submitted on 4 Nov 2019

Determination of the copper isotope composition of seawater revisited: A case study from the Mediterranean Sea

Isabelle Baconnais[1,2]*, Olivier Rouxel[2,3], Gabriel Dulaquais [4], Marie Boye [4,5]

[1] University of Saskatchewan - Saskatoon, Canada.

[2] IFREMER, Centre de Brest, Technopôle Brest Iroise - Plouzané, France.

[3] Department of Oceanography, University of Hawaii, Honolulu, USA

[4] Laboratoire des sciences de l'environnement marin, UMR CNRS 6539, Institut Universitaire Européen de la Mer, Université de Bretagne Occidentale - Plouzané, France

[5] Laboratoire d'océanographie et du climat expérimentation et approches numériques, UMR CNRS 7159, Université Pierre et Marie Curie - Paris, France

Marine Chemistry

*Corresponding author. Email: isabelle.baconnais@usask.ca

1   **Abstract**

2   A new technique for the determination of dissolved copper isotope composition (δ^{65}Cu) of

3   seawater was applied to examine copper sources and internal cycling in the Mediterranean Sea.

4   A succession of chelating resin with nitrilotriacetic acid functional groups and strong base

5   anion exchange resin, together with optimization of the multi-collector inductively coupled

6   plasma mass spectrometry set-up allowed to isolate copper from seawater matrix and to

7   measure the ^{65}Cu/^{63}Cu ratios in seawater with an external precision of 0.06 ‰ (2 s.d.). This

8   method was first applied for inter-comparison measurements to surface and deep waters

9   sampled at station BATS in the North Atlantic Ocean. Disparities in δ^{65}Cu reported here and

10   in the literature over these samples showed a need to investigate whether a new inter-

11   comparison sample should be decided upon, or whether the use of UV-oxidation can also affect

12   the measurement of δ^{65}Cu. We also measured total dissolved Cu concentration ([dCu]$_T$) and

13   δ^{65}Cu for 12 stations in the Mediterranean Sea. The δ^{65}Cu distribution showed significant

14   variations in the euphotic zone, at the Chl *a* maximum and at bottom depths. Copper isotope

15   ratios ranged from +0.21 ‰ to +0.76 ‰ (± 0.06 ‰, 2 s.d.), yielding an average of +0.51 ‰ (±

16   0.20 ‰, 2 s.d.; n = 96) for the Mediterranean Sea. A strong zonation between natural aerosol

17   deposition to the South and anthropogenic aerosol deposition to the North was seen in the

18   sample set (Dulaquais et al., 2017; Gerringa et al., 2017; Rolison et al., 2015). Natural dust

19   deposits seemed to draw δ^{65}Cu toward lower values and deeper in the euphotic zone whereas

20   the impact of anthropogenic aerosols seemed restricted to an increase in [dCu]$_T$. At the Chl *a*

21   maximum, δ^{65}Cu showed significant increase which we attributed to scavenging on and/or

22   uptake by phytoplankton. The isotope signature of Cu sources to the Mediterranean Sea were

23   also investigated and we inferred a significant source of isotopically heavy Cu in the Gibraltar

24   area, potentially originating from a release of Cu sulfide leached in the mining area of Southern

25   Spain (*i.e.* Iberian Pyrite Belt) in rivers and transported to the Mediterranean Sea in surface by

1 seasonal water mass circulation. Conversely, marine sediments appear to be a source of

2 isotopically-light Cu to deep waters. This study provides new hints on the use of copper

3 isotopes to study sources and sinks of Cu in seawater.

4 **<Keywords>** Copper isotope; seawater; Mediterranean Sea; Geotraces; isotope fractionation

1　**1. Introduction**

2　Copper (Cu) is a key micro nutrient in seawater that contributes to photosynthesis,

3　denitrification and iron uptake by primary producers in the food chain (Peers and Price, 2006;

4　Peers et al., 2005; Zumft and Kroneck, 2007), but that exerts acute toxic effects on

5　phytoplankton above a free Cu^{2+} level of 0.01 nmol kg^{-1} (Moffett et al., 1997). Studies have

6　found that above this critical Cu^{2+} level, both prokaryotic and eukaryotic phytoplankton species

7　release strong Cu complexing agents in cultures as an effective detoxification mechanism

8　(Croot et al., 2000; Moffett and Brand, 1996; Rue and Bruland, 2001). This process might be

9　the reason for the dissolved pool of Cu being mostly governed by organic complexation (95 –

10　99.8 %) in seawater (Coale and Bruland, 1988; Moffett and Dupont, 2007), although some

11　eukaryotes are able to access the organically complexed pool of Cu (Semeniuk et al., 2015;

12　Semeniuk et al., 2009). Total dissolved Cu concentrations ($[dCu]_T$) in seawater ranges from

13　0.3 nmol kg^{-1} to 7.6 nmol kg^{-1} (Bruland and Franks, 1983; Thompson and Ellwood, 2014;

14　Vance et al., 2008) and Cu has a nutrient-like profile with relatively low surface concentrations

15　increasing with depth. This distribution is explained by plankton uptake in surface,

16　remineralization at intermediate depths and deep-water accumulation to which is added a

17　significant sedimentary benthic source (Jacquot and Moffett, 2015; Roshan and Wu, 2015;

18　Saager et al., 1992; Takano et al., 2014). A modeling study suggests that below the photic zone,

19　dissolved Cu (dCu) is at equilibrium with falling particles and exchanges reversibly between

20　dissolved and adsorbed state (Little et al., 2013). This process is called reversible scavenging.

21　Copper has two naturally occurring stable isotopes: ^{63}Cu (69.17%) and ^{65}Cu (30.83%). Natural

22　mass-dependent variations in $^{65}Cu/^{63}Cu$ span 15‰, expressed relative to the NIST SRM 976

23　standard as $\delta^{65}Cu$ values (recently reviewed in Moynier et al., 2017).

24　$$\delta^{65}Cu = \left[\frac{(^{65}Cu/^{63}Cu)_{sample}}{(^{65}Cu/^{63}Cu)_{SRM\ 976}} - 1\right] \times 1000.$$

1 Initial studies of Cu isotope fractionation in natural systems demonstrated the great potential

2 of Cu isotopes as new tracers for the study of modern and ancient hydrothermal systems and

3 ore deposits (Graham et al., 2004; Larson et al., 2003; Maher and Larson, 2007; Marechal et

4 al., 1999; Mason et al., 2005; Rouxel et al., 2004; Zhu et al., 2000). So far, experimental and

5 field studies have indicated that redox transformations between Cu(I) and Cu(II) species are

6 the main processes resulting in Cu isotope fractionation in natural systems (Ehrlich et al., 2004;

7 Mathur et al., 2005; Zhu et al., 2002). Reduced and precipitated Cu(I) species are known to be

8 lighter by 2 to 5 ‰ relative to dissolved Cu(II) species (Ehrlich et al., 2004; Fujii et al., 2013;

9 Mathur et al., 2005; Sherman, 2013; Zhu et al., 2002). Because Cu speciation in seawater is

10 dominated by Cu^{2+} complexation with organic ligands (Coale and Bruland, 1988; Moffett et

11 al., 1990), changes in Cu speciation in aqueous systems may also lead to significant Cu isotope

12 fractionation (Fujii et al., 2013), with fractionation between organically complexed dCu and

13 free inorganic dCu ($\Delta^{65}Cu_{complex-free}$) of +0.1 to +0.8 ‰ (Bigalke et al., 2010; Ryan et al., 2014).

14 Recent studies have made an effort to measure the isotope ratio of Cu in seawater and its

15 sources and sinks. In a reconnaissance study, Vance et al. (2008) reported a relatively large

16 range of dissolved $\delta^{65}Cu$ between +0.02 and +1.45 ‰ in rivers and estuaries. Although the

17 underlying mechanisms of Cu isotope fractionation in weathering environments remain

18 unclear, isotopically heavy dissolved $\delta^{65}Cu$ in rivers likely results from a balance between the

19 preferential partitioning of light Cu isotopes into soils and suspended particles (Bigalke et al.,

20 2010; Bigalke et al., 2011), with varying fractionation factors according to the importance of

21 the mineral fraction in the soil (Babcsanyi et al., 2016), and the remobilization of isotopically

22 light Cu(I) and reduced Cu from (and within) the sediments in a run-off (Babcsanyi et al.,

23 2014). Other studies further suggest that Cu isotope fractionation could be useful tracers of Cu

24 biogeochemical cycling. For example, Zhu et al. (2002) reported that the reduction and

25 incorporation of Cu(II) within protein and yeast cells may lead to significant Cu isotope

1 fractionation ($\Delta^{65}Cu_{protein/yeast-source}$ from -1.7 ‰ to -1.0 ‰) due to the incorporation of light

2 isotopes as Cu(I) species. The preferential uptake or adsorption of heavy Cu isotopes onto

3 common soil and aquatic bacteria, and marine and freshwater diatoms has been also reported,

4 with fractionations of up to +5.6 ‰ (Mathur et al., 2005; Pokrovsky et al., 2008). However,

5 the direction and extent of Cu isotope fractionation during Cu adsorption on organic matter-

6 rich particles and absorption on cells remain unclear, however, and likely depend on Cu

7 bonding environments and kinetic vs. equilibrium effects (Navarrete et al. (2011).

8 The study of the isotope fractionation of marine dCu is relatively new. The first dataset of

9 dissolved $\delta^{65}Cu$ in seawater from the Pacific Ocean, Indian Ocean and English Channel was

10 published by Vance et al. (2008) and reported $\delta^{65}Cu$ values ranging from +0.9 to +1.4 ‰ ($\pm$

11 0.1 ‰, 2 s.d.) indicating that dissolved $\delta^{65}Cu$ generally exhibits higher values in open ocean

12 than in riverine systems. More recently, Thompson et al. (2014) investigated the distribution

13 of Cu isotope ratios along three vertical profiles in contrasted biogeochemical domains of the

14 Pacific Ocean to address variations in $\delta^{65}Cu$ according to marine productivity. However, only

15 minor differences of the average $\delta^{65}Cu$ were observed between the stations (from +0.61 $\pm$ 0.16

16 ‰ to +0.78 $\pm$ 0.16 ‰). Takano et al. (2014) also investigated several profiles in the Pacific and

17 focused mostly on surface layers, emphasizing the role of atmospheric deposition and surface

18 biogeochemical processes. The overall variation of $\delta^{65}Cu$ in deep and surface waters observed

19 was +0.41 to +0.85 ‰, and the authors proposed that $\delta^{65}Cu$ becomes heavier along the oceanic

20 circulation because of preferential scavenging of ^{63}Cu. The heavy isotope composition of the

21 ocean likely results from internal processes, possibly due to isotopic partitioning between an

22 isotopically light pool adsorbed onto particles and a heavy dissolved pool strongly bound to

23 organic ligands (Little et al., 2014; Vance et al., 2008).

24

1   In order to further understand Cu isotope fractionation in seawater, it is necessary to gather a

2   larger dataset of $\delta^{65}Cu$ encompassing several Cu sources and sinks, as well as different oceanic

3   water masses and contrasting biogeochemical domains. The Mediterranean Sea is an

4   advantageous location for this exercise, considering the semi-enclosed formation of the sea and

5   the relatively extensive knowledge of its water masses and continental inputs (Bethoux, 1980;

6   Millot and Taupier-Letage, 2005; Robinson et al., 2001). The Mediterranean Sea is also well-

7   known for its enrichment in trace elements compared to the Atlantic Ocean, and its influence

8   on the Atlantic Ocean budget of dissolved trace-metals (Boyle et al., 1985; Van Geen and

9   Boyle, 1990; Van Geen, 1989).

10   In June/July 2013, the GEOTRACES-A04N section was conducted to constrain the

11   distribution of bio-essential and other trace elements and isotope ratios in the Mediterranean

12   and Black Seas (Rijkenberg, 2013a). Using an improved method, we present in this study the

13   first isotope composition of dCu in the Mediterranean Sea from samples collected along this

14   section. The analytical method allowed the separation of total dissolved Cu at low pH (1.8)

15   from 1 L of seawater and its application to a set of inter-comparison seawater samples,

16   including the GEOTRACES BATS samples (Boyle et al., 2012). Potential isobaric

17   interferences and matrix effects on MC-ICP-MS were also investigated. We then report the

18   distribution of dissolved $\delta^{65}Cu$ through the water column of the Mediterranean Sea, and studied

19   the variations of $\delta^{65}Cu$ in relationship with hydrographic and biogeochemical parameters.

20

21   **2. The Mediterranean Sea**

22   **2.1 Sampling**

23   The cruise was conducted on the RV Pelagia from May to August 2013 along the

24   Geotraces-A04N transect in the Mediterranean Sea (Figure 1). Seawater samples were

1   collected using the TITAN-CTD frame of the NIOZ, the Royal Netherlands Institute for Sea

2   Research(De Baar et al., 2008), equipped with 24 ultra-clean sampling bottles of 24 L each

3   made of polyvinylidene (PVDF) and titanium (Rijkenberg, 2013a; Rijkenberg, 2013b). After

4   deployment, the TITAN system was moved to a Class-100 container for sub-sampling.

5   Samples were filtered in-line under N_2 pressure (filtered 99.99% N_2, 0.7 atm) at 0.2 µm using

6   Sartobran 300 cartridges (Sartorius®). Filtered seawater samples were stored in 1L LDPE

7   bottles (Nalgene®) previously cleaned following the GEOTRACES procedure for trace metal

8   analysis (Cutter et al., 2014).

9   Hydrographic parameters (*e.g.* dissolved oxygen, temperature, salinity, density) were acquired

10   using a CTD-package. As described in Gerringa et al. (2017), it consisted of a SeaBird SBE9

11   plus underwater unit, a SBE11plusV2 deck unit, a SBE3plus temperature sensor, a SBE4

12   conductivity sensor, a Wetlabs C-Star transmissometer (25 cm, deep, red) and a SBE43

13   dissolved oxygen sensor. Fluorescence was measured as the beam attenuation coefficient at

14   660 nm using a Chelsea Aquatracka MKIII fluorometer. The fluorometer signal was calibrated

15   against Chlorophyll *a* and is expressed as mg Chl *a*. m^{-3}. Oceanographic parameters were

16   standardized following the Thermodynamic Equation Of Seawater - 2010 (TEOS-10) agreed

17   upon by the Intergovernmental Oceanographic Commission (IOC), such as salinity and

18   temperature are expressed as Absolute Salinity (S_A in g kg^{-1}) and Conservative Temperature

19   (CT in °C) using the Gibbs Sea Water (GSW) program (McDougall and Barker, 2011). Maps

20   and transects were made using ODV (Schlitzer, 2016).

21

22   **2.2. Study area**

23   The Mediterranean Sea is a semi-enclosed basin subject to strong evaporation (Mariotti et al.,

24   2002), with distinct water masses showing contrasting salinity (figure 2). The Mediterranean

25   Sea nests local hydrographic anomalies, such as the occurrence of eddies (Richardson et al.,

1   2000), the formation of dense waters in the Gulf of Lion and in the southern Aegean Sea (Millot

2   and Taupier-Letage, 2005), or the presence of anoxic brines in the Tyro and Bannock basins

3   (Saager et al., 1993). The dynamic of the Mediterranean Sea is illustrated by the short residence

4   time of the water masses, which is about 15 years for the Western Mediterranean basin and 50

5   years for the Eastern basin (Laubier, 2005). We expect this particularity to help constraining

6   the sources and sinks of Cu rather than the long-term processes of scavenging typical of the

7   open-ocean (Bruland and Franks, 1983).

8   The hydrography of the section was described by van Aken (2015) and other recent studies

9   (Dulaquais et al., 2017; Gerringa et al., 2017; Rolison et al., 2015).

10   The Atlantic Ocean was sampled from stations 1 to 4 (Fig. 1 and 2). Surface Atlantic Water

11   (SAW) flowing from 0 m to 200 m is a relatively warm, saline water mass ($\sigma_\theta < 27.2$ kg m^{-3};

12   $S_A > 36.3$ g kg^{-1}; Fig. 2) entering the Mediterranean Sea above North Atlantic Central Waters

13   (NACW) (Gascard and Richez, 1985). The underlying core of NACW flows from 200 m to

14   500 m ($S_A < 36.3$ g kg^{-1}; Fig. 2). Mediterranean Sea Outflow Water (MSOW) is the result of

15   warm and saline Mediterranean seawater leaking through the Gibraltar Strait and mixing with

16   fresher surface waters in the Gulf of Cadiz (Ambar and Howe, 1979; Coste et al., 1988; Howe,

17   1982). It is an intermediate water mass leaking into the North-East Atlantic Ocean between

18   750 m and 1250 m ($\sigma_\theta = 27.4$ to 27.8 kg m^{-3}; $S_A > 36.0$ g kg^{-1}) (Zenk and Armi, 1990). Below

19   MSOW, North-East Atlantic Deep Water (NEADW) is observed between 1500 m to 2500 m

20   ($\sigma_\theta = 27.9$ kg m^{-3}; $S_A = 35.2$ to 36.0 g kg^{-1}) with underlying Lower Deep Water (LDW) from

21   2500 m to the bottom ($\sigma_\theta = 27.9$ kg m^{-3}; $S_A \sim 35.0 - 35.1$ g kg^{-1}) (Van Aken, 2015).

22   The cold, less saline Atlantic waters enter the Mediterranean Sea in surface through the

23   Gibraltar Strait, and can be seen at station 5S from surface to ~130 m (Fig. 2). Atlantic water

24   travels in surface of the Mediterranean Sea and is progressively modified within the Western

25   Mediterranean basins (WMB) to form Modified Atlantic Water (MAW) (Robinson et al., 1992;

1   Send et al., 1999), where it lies at stations 11S, 12N and 17N above 100 m with S_A between

2   37.2 g kg^{-1} and 38.2 g kg^{-1} (Fig. 2). MAW extends in surface to the Eastern Mediterranean

3   Basin (EMB) at shallower depths, with an increasing salinity of < 38.8 g kg^{-1} (station 21, above

4   70 m; Fig. 2), describing a counter-clockwise circulation pattern along the continental coast

5   (Millot and Taupier-Letage, 2005).

6   Levantine Intermediate Water (LIW), formed in the EMB, is the most saline water mass (CT

7   >14°C; S_A > 39.0 g kg^{-1}) in the Mediterranean Sea, and is poorer in nutrients and oxygen than

8   MAW (Millot and Taupier-Letage, 2005; Rolison et al., 2015). Within the EMB, the southern

9   stations 18S and 21S are affected by the LIW between 70 m and 500 m, whereas the northern

10   stations 5N and 9N are affected from the surface to 800 m (Fig. 2). LIW is formed in winter

11   close to the isle of Rhodes in the EMB (Millot and Taupier-Letage, 2005) and circulates

12   counter-clockwise around the EMB, partially infiltrating the southern Adriatic Sea where

13   station 9N lies, to form in winter a dense, also saline (S_A < 38.9 g kg^{-1}) deep water mass,

14   Adriatic Deep Water (AdDW) (Millot and Taupier-Letage, 2005). The rest of LIW continues

15   flowing in the Tyrrhenian Sea through the Strait of Sicily and returns to the EMB (Millot and

16   Taupier-Letage, 2005). Traces of LIW can be seen between 250 m and 1000 m at stations 11S

17   and 17N with S_A > 38.7 g kg^{-1} (Gerringa et al., 2017). In each basin (WMB and EMB) exists a

18   deeper water mass with unique hydrographic characteristics. Eastern Mediterranean Deep

19   Water (EMDW) fills the EMB with S_A around 38.9 g kg^{-1}, affecting stations 18S, 21S, 5N and

20   9N below 500 m (Fig. 2). Western Mediterranean Deep Water (WMDW) fills the deep levels

21   of the WMB (Send et al., 1999), affecting stations 5S, 11S and 17N between 150 m and the

22   intrusion of LIW, and below 1000 m to bottom with S_A around 38.7 g kg^{-1}.

23   The main sources of freshwater to the Mediterranean Sea are limited to the Po (Italy), the Tiber

24   (Spain), the Rhône and Ebro rivers (France), and the Nile (Egypt) (Ludwig et al., 2009). Dust

25   input to the nutrient-depleted Mediterranean Sea is considerable in quantity and effect (Duce

1   and Tindale, 1991; Goudie and Middleton, 2001; Guieu et al., 1991; Herut et al., 2005; Jordi

2   et al., 2012; Ternon et al., 2011) and it is thus a natural laboratory to study the consequences

3   of dust deposition on the surface ocean (Coale et al., 1996). A study by Jordi et al. (2012)

4   showed that pulses of this large dust deposition in surface water are responsible for inhibiting

5   the growth of phytoplankton population, especially considering that the atmospheric input of

6   dissolved Cu to the Mediterranean basins is up to 5 times the flux of riverine inputs (Guerzoni

7   et al., 1999).

8

9   3. Analytical Method.

10   3.1 Chromatographic separation.

11   The seawater samples were filtered through 0.2 μm, therefore we measured the dissolved

12   fraction of Cu plus the labile fraction from fine particles under 0.2 μm. In this study, both

13   fractions fall under the appellation dCu for simplicity. Seawater samples were then acidified to

14   pH=1.7 using ultrapure HCl (Optima^{TM}) in a clean shore-based laboratory. Optima-grade H_2O_2

15   was added to 0.03 wt% to enhance the dissociation of organic ligands and labile Cu(II).

16   Samples were then left aside in the dark for 2 - 4 months before being processed.

17   Preparation and chromatographic purification of the samples are summarized in Table 1. All

18   manipulations were conducted in a Class 1000 (ISO 6) clean room and all samples were

19   handled inside a Class 100 (ISO 5) laminar flow hood. All Teflon and LDPE vials were acid-

20   leached prior to use. All reagents were prepared gravimetrically using distilled analytical grade

21   acids and ultrapure water (Milli-Q®, 18.2 MΩ). Procedural blanks and chemistry yields were

22   assessed for each sample batch (*i.e.* for every 12 samples) by processing 100 ng of Cu standard

23   NIST SRM 3114.

1   All steps of the chemistry are summarized in Table 1. Copper pre-concentration and extraction

2   from seawater followed a method using nitrilotriacetic acid resin (NTA Superflow®,

3   Qiagen™), which was previously used for measuring Fe isotope fractionation in seawater by

4   Rouxel and Auro (2010), and was adapted from the protocol of Lohan et al. (2005). The pre-

5   concentration process was accelerated by using a peristaltic pump set to draw seawater at a

6   constant flow rate of 10 mL min^{-1} during conditioning and elution of the seawater matrix.

7   After recovery of the eluted sample on NTA, an aliquot of 0.4 mL was pipetted from the

8   recovered sample and diluted to 20% using 18.2 MΩ water for preliminary Cu concentration

9   determination on Multi-Collector Inductively Coupled Plasma Mass Spectrometer (MC ICP-

10   MS).

11   A macroporous strong base anion exchange resin AG MP-1M (100-200 mesh) (Bio Rad Inc.)

12   was used for further separation of Cu from remaining elements, in particular Fe. The method

13   essentially followed previously-established methods described in Borrok et al. (2007) and

14   Marechal et al. (1999) (Table 1). The Cu fraction recovered from the AG MP-1M resin was

15   dried down and re-dissolved in concentrated Optima™-Grade HNO$_3$, put back to evaporation

16   before being finally dissolved in an adjusted volume of 0.28M HNO$_3$ to obtain a final

17   concentration for Cu of about 100 ng mL^{-1}.

18   **3.2. Determination of Cu isotope ratios by Multicollector ICPMS.**

19   Cu concentrations and isotope ratios were analyzed using a Thermo Scientific™ Neptune

20   Multi-collector (MC) ICPMS operated at Ifremer-Brest. The instrument was used in low mass

21   resolution mode with high-efficiency sampler cones (Ni X-cones), and a double-pass spray

22   chamber as the introduction system.

23   For each sample, the pre-determination of Cu concentration on MC-ICPMS using a 4% aliquot

24   was necessary to adjust the concentration of the samples to ~100 ng mL^{-1} (± 20 ng mL^{-1}) prior

1   to analysis. This step allowed a more precise determination of $\delta^{65}Cu$ and $[dCu]_T$, as all

2   measurements were bracketed with a standard Cu NIST SRM 976 (100 ng mL^{-1}).

3   Cu isotope ratios and concentrations were simultaneously measured on MC-ICPMS. Each

4   sequence of measurement was repeated 3 to 6 times, and only average $\delta^{65}Cu$ values were

5   reported for each sample. Internal precision was calculated as the 2 Standard Deviation (s.d.)

6   of the mean. Under typical analytical conditions, an internal precision better than 0.10 ‰ (2

7   s.d.) was obtained, while repeated analysis of standard NIST SRM976 gave an instrumental

8   external precision of 0.06 ‰ on $\delta^{65}Cu$ values at 95% confidence (2 s.d.; n=638). Hence, when

9   an internal precision (2 s.d.) better than 0.06 ‰ was obtained, we applied the external precision

10   to report analytical uncertainty. Multi-elemental standard solutions were used for instrumental

11   calibration and Cu concentrations were determined within 5% relative s.d..

12   Surface (GS) and deep (GD) seawater samples from the GEOTRACES inter-comparison

13   stations of BATS (North Atlantic; Boyle et al.(2012)) were processed to determine the accuracy

14   of the method.

15   **4. Results**

16   **4.1. Isobaric interference of ZnH on ^{65}Cu.**

17   Over the course of the development of the method, we used a Zn standard solution (SRM3168a

18   solution) to correct for instrumental mass bias as widely used in previous studies (Albarede,

19   2004; Archer and Vance, 2004; Fujii et al., 2013; Marechal et al., 1999; Takano et al., 2013).

20   This approach was however discontinued due to potential formation of Zn-hydride

21   interferences on Cu isotopes. Using a desolvation nebulizer (Apex-Q; ESI), we determined the

22   percentage of Zn hydride formation ($^{64}ZnH/^{64}Zn$) to be about 0.007 %. Because of the relatively

23   large correction factor (up to 1.35‰) for solutions with high Zn/Cu ratios, which is typically

24   the case when measuring low-concentration Cu isotope ratios, we decided to avoid the use of

1   Zn as an internal standard for instrumental mass bias correction. In a previous study, Mason et

2   al. (2004) also reported the occurrence of a Zn-hydride interference on m/z (mass-to-charge

3   ratio = 65) leading to shifts in $^{65}Cu/^{63}Cu$ measurement.

4.2. Matrix effects and matrix-induced isobaric interferences.

5   Isobaric interferences on Cu isotopes may involve double-charged ions (Ba^{2+}), argides ($NaAr^+$,

6    $MgAr^+$), and oxides ($NaOH^+$, TiO^+, $TiOH^+$, PO_2^+, SO_2^+, SO_2H^+, $CaOH^+$, $ClNO^+$) (May and

7   Wiedmeyer, 1998). In the case of seawater analysis, Na-based, Mg-based, Cl-based and S-

8   based ions are the most critical potential interferences. Hence, the chemical purification step is

9   essential to avoid spectral and non-spectral interferences on MC-ICPMS. As discussed

10   previously (Rouxel and Auro, 2010), the pre-concentration method using NTA resin removes

11   most of these matrix elements, but an additional purification step using anion resin is often

12   required to achieve the highest purification level. Several approaches were used to verify the

13   achievement of interference-free measurements: (1) using the high-mass resolution capability

14   of the Neptune MC-ICPMS, we checked the absence of remaining oxide and argide-based

15   interferences on Cu isotopes spectra; (2) measurement of $\delta^{65}Cu$ on Cu-doped ultra-pure water

16   gave consistent results (see section 4.3). We also measured Ca and Mg concentrations in

17   processed seawater samples to control for the absence of remaining seawater matrix elements.

18   The formation of matrix-related polyatomic species during sample preparation and their

19   introduction into the mass spectrometer may also induce non-spectral interferences. Such

20   interferences are often referred to as matrix effects, whereby ionization efficiency and

21   instrumental mass bias of the analyte are modified by the presence of other matrix elements.

22   Over the course of the method development, we observed significant shifts in the Cu isotope

23   ratio of the Cu standard ultrapure water solution when processed through the chemistry. Hence,

24   we further investigated possible matrix effects generated by the method.

1 Several ultrapure water samples were processed through the entire chemistry and enriched with

2 Cu SRM976 prior to analysis. In a first set of experiments, a desolvating nebulizer Apex-Q

3 (ESI[TM]) was used as introduction system and instrumental mass bias was corrected using a

4 sample-standard bracketing approach. A Ni standard solution was also used as external

5 standard to further monitor instrumental mass bias. Results showed systematic negative shifts

6 of the corrected δ^{65}Cu values down to -1.7‰ (Fig. 3), which cannot be explained by changes

7 in instrumental mass bias since Ni isotope ratios remained identical within uncertainties

8 between the samples and bracketing standard solutions (Fig. 4). This suggests that either Cu is

9 the only element prone to significant matrix effects (*e.g.* complexation or redox effects), or that

10 the mass 63 is affected by significant isobaric interferences. In a second set of experiments, a

11 conventional cyclonic spray chamber was used instead of desolvating nebulizer and

12 instrumental mass fractionation was corrected using a sample-standard bracketing approach.

13 Results show, considering uncertainties, identical δ^{65}Cu values between processed and

14 unprocessed standard **(**Fig. 3**)**. Hence, we propose that the dryer and hotter plasma conditions

15 and/or the desolvating process itself are responsible for the large shift in Cu isotope ratio.

16 Archer and Vance (2004) already described sudden instrumental mass bias shifts when using a

17 desolvating nebulizer which could not be corrected by the use of Zn internal standard. While

18 they suggested that a change in Cu oxidation state could have occurred within the introduction

19 system, leading to its adsorption on the desolvating membrane, Bermin et al.(2006) later

20 suggested either a mass bias artifact or the enhancement of interferences on elements in the

21 matrix other than Cu (*e.g.* ^{66}Zn). In the first experiment set using desolvating nebuliser, the

22 shift in δ^{65}Cu was observed regardless of the instrumental mass bias correction method (i.e.

23 external normalization to Ni or sample-standard bracketing), which implies Cu-specific

24 interferences enhanced by the desolvating mechanism. We propose that such interferences

25 arose from the presence of refractory organic matrices produced during the chemical

1   purification steps that affected the behavior of Cu during desolvation. Post-column treatment

2   of the samples with concentrated HNO_3 and H_2O_2 did not remove such interferences.

3   Therefore, despite the lower sensitivity (decreased by a factor of 2.5), we used a cyclonic spray

4   chamber as sample introduction system, combined with a standard-sample-standard method to

5   limit extensive corrections and/or interferences. In addition, the use of Ni or Zn as internal

6   standard did not result in enhanced precision compared to a conventional standard-sample

7   bracketing approach.

8   **4.3. Procedural blanks, yield and external reproducibility**

9   Concentrations of Cu, Ni and Zn were measured on each procedural blanks and sample

10   solutions for contamination control. Procedural blanks were estimated by using 1 L of ultra-

11   pure water acidified to pH 1.8 and passed through the entire process. The resulting Cu blanks

12   mostly ranged between 2.2 ng and 3.7 ng (n = 5), and therefore account for less than 2.4 % of

13   typical open-ocean Cu concentrations.

14   The yield for Cu recovery was assessed using a standard-addition method. This approach has

15   been already used in several metal isotope fractionation studies in seawater (Rouxel and Auro,

16   2010; Takano et al., 2013). It consists in adding incremental amounts of a standard solution of

17   known concentration and isotope ratios, in this case Cu SRM3114 to an unknown seawater

18   sample. Here, we used an open deep Pacific seawater sample sampled recovered off Hawaii

19   (cruise KM0923, October 2009). The relationships between measured $\delta^{65}Cu$ values and the

20   percentage of Cu added to the composite samples are shown in Fig. 5. The correlation line

21   defines two end-members: (1) $\delta^{65}Cu$ of the standard SRM3114 at the intercept, *i.e.* -0.06 ± 0.02

22   ‰ (2s.e.); (2) $\delta^{65}Cu$ of the seawater sample, extrapolated at 100% (*i.e.* Cu_{sw}/Cu_{mes} = 1) and

23   measured at 0.50 ± 0.08 ‰ (2s.d.). Previous value for the intercept was calculated using the

24   least square function LINEST (Excel, Microsoft), and associated error was adapted to be at

1   2s.e.. Considering that SRM3114 has a $\delta^{65}Cu$ value of -0.054 ± 0.05 ‰ (2s.d.; n=7), the

2   standard addition method gave consistent results. When comparing concentration of total Cu

3   measured *vs*. the theoretical concentration of Cu SRM3114 used, we determined a recovery of

4   Cu on the NTA resin of about 96.5% (± 5%). Copper concentration in the bulk seawater was

5   measured at 0.48 ± 0.01 nmol kg^{-1}, which is consistent with published values for North Pacific

6   surface water (Biller and Bruland, 2012; Bruland, 1980). Hence, it can be suggested that the

7   chemical procedure does not fractionate Cu, even though this method may not fully recover

8   about 5% of Cu initially present in the sample.

9   Due to the limited volume of seawater available for the study, the external reproducibility could

10   not be determined via replication of seawater samples. Instead, we measured replicates of ultra-

11   pure water enriched with Cu standard SRM3114. The average $\delta^{65}Cu$ determined was -0.10 ±

12   0.06 ‰ (2 s.d.; n=12), giving a precision for the method of 0.06‰. This result is similar to the

13   non-processed $\delta^{65}Cu$ value of SRM 3114 ($\delta^{65}Cu$ = -0.06 ± 0.02 ‰, 2 s.d., n=44).

14   **4.4. Inter-comparison samples**

15   We processed two GEOTRACES North Atlantic Inter-calibration 2008 reference samples from

16   the Bermuda Station, surface and deep water (respectively GS and GD), for which $[dCu]_T$

17   consensus values agreed upon by 10 different laboratories using various methods are available

18   at

19   https://websites.pmc.ucsc.edu/~kbruland/GeotracesSaFe/2012GeotracesSAFeValues/GEOTR

20   ACES_Ref_Cu.pdf. As part of the inter-comparison exercise, $\delta^{65}Cu$ was measured on these

21   samples by Boyle et al. (2012) and Takano et al. (2014) (Table 2).

22   The values for $[dCu]_T$ and $\delta^{65}Cu$ obtained using our method are very similar between the

23   Atlantic station 1 and our measurements of BATS samples. The surface samples gave $[dCu]_T$

1   of 0.8 - 0.9 nmol kg^{-1} with $\delta^{65}Cu$ of +0.4 ‰, and the deep seawater samples displayed higher

2   values for [dCu]$_T$ (1.38 nmol kg^{-1}) and $\delta^{65}Cu$ (+0.6 ‰) (Table 2).

3   Some disparities appeared when comparing our data to the GEOTRACES consensus values.

4   We measured [dCu]$_T$ at a concentration 11 – 15 % inferior to the consensus values for GD, and

5    $\delta^{65}Cu$ ~30 % lighter than that measured by Boyle et al. (2012) for GS and ~50% heavier than

6   that measured by Takano et al. (2014) for GD.

7   Recent studies focussed on the effect of UV-oxidation pre-treatment on the variability in

8   [dCu]$_T$ in seawater samples (Middag et al., 2015; Posacka et al., 2017). As numerous authors

9   demonstrated, *e.g.* Milne et al. (2010), Biller and Bruland (2012), 1hr of UV-oxidation

10   increases [dCu]$_T$ by ~10% by breaking down organic metal-binding ligands, which motivated

11   a new assessment of the consensus values for GS and GD (Table 2). However, Posacka et al.

12   (2017) showed that UV-oxidation is mostly effective on [dCu]$_T$ in samples acidified less than

13   2 months prior to analysis, and suggest that UV-oxidation might not be necessary for samples

14   stored for a long period of time (*i.e.* $\geq$ 4 years). In this study, our inter-comparison samples GS

15   (~7 m) and GD (~2000 m) were acidified and stored for 6 years prior to analysis, and [dCu]$_T$

16   reported for GS is similar between our study and the 2011 and 2013 consensus values (Table

17   2). All BATS samples GS and GD from 2008 are exhausted, so the discrepancy in [dCu]$_T$

18   between our deep-water sample GD and the consensus values cannot be investigated.

19   Therefore, we do not dismiss the possibility that in our GD sample, Cu-binding ligands were

20   not quantitatively broken down by an extensive period of storage at low pH and addition of

21   H_2O_2. Thompson et al. (2013) also tested the impact of UV-oxidation and addition of H_2O_2

22   prior to extraction with no conclusive effect on $\delta^{65}Cu$ compared to un-manipulated samples.

23   Authors Little et al. (2018) report variations up to ~30% in [dCu]$_T$ between a measurement via

24   UV-High resolution technique, and a measurement via beam matching with standards of known

25   concentration (similar to this study), and confirm the absence of significant effect on $\delta^{65}Cu$.

1   At the moment, we cannot further investigate the discrepancies in $[dCu]_T$ and $\delta^{65}Cu$ between

2   our data and reported values, for the reasons mentioned earlier. Increased collaboration

3   between laboratories would be necessary to determine whether the samples used as inter-

4   comparison were not homogeneous or whether there are analytical issues to be overcome.

5   In this study, $[dCu]_T$ is reported within 10% error, taking into account the possible non-

6   quantitative degradation of organic ligands and dCu. Furthermore, standard addition test and

7   comparison to literature gives us confidence in our isotopic data.

8   **4.5. Dissolved Cu concentration and isotope ratio in the Mediterranean Sea**

9   We investigated the distribution of Cu concentrations and isotope ratios of 97 samples

10 from 11 stations across the Mediterranean Sea, representing a subset of seawater samples

11 collected during the GEOTRACES-A04N cruise. Depth resolution varied anywhere from 10

12 m to 1000 m and sampling depths were selected to capture the main hydrographic structures.

13 All data and complementary hydrographic parameters are available in Table 3.

14 Dissolved Cu concentrations varied between 0.72 nmol kg^{-1} (station 3; 75m) and 6.00 nmol kg^{-1}

15 ^{1} (station 9N; 10m). Most of the variations occurred above 200 m and near the benthic layer.

16 Seawater below 200 m displayed an eastward increase in average $[dCu]_T$, from 1.27 nmol kg^{-1}

17 ($\pm$ 0.51 nmol kg^{-1}, 1s.d.; n = 10) in the Atlantic to 1.91 nmol kg^{-1} ($\pm$ 0.40 nmol kg^{-1}, 1s.d.; n =

18 16) in the EMB.

19 High $[dCu]_T$ were measured at stations 5S (10 m), 11S (40 m), 21S (85 m) and 9N (10 m). In

20 the Alboran Sea (station 5S), $[dCu]_T$ in the inflowing Atlantic seawater (surface to 130 m) is

21 about 2 to 3 times the concentration found at similar depths in the Atlantic stations 1 to 4, with

22 a corresponding $\delta^{65}Cu$ up to +0.68 ‰. Comparatively high surface $[dCu]_T$ was reported by Van

23 Geen (1989) at a similar location in the Alboran Sea. Surface waters at station 11S were

24 affected by heavy rains and eddies during sampling (Dulaquais et al., subm.), possibly

1   explaining the peculiar sub-surface $[dCu]_T$ maxima of 4.30 nmol kg^{-1} and $\delta^{65}Cu$ minima of

2   +0.23 ‰ measured at 40 m. The highest $[dCu]_T$ in the Mediterranean Sea is found at station

3   9N in surface water (6.00 nmol kg^{-1}), for which high concentrations of dissolved Cu and other

4   trace elements (*e.g.* Zn, Mn, Co) have been observed at a similar depth (Zago et al., 2002). We

5   do not have an explanation for the high $[dCu]_T$ observed at Chl *a* maximum at station 21S, and

6   do not exclude the possibility of contamination of the sample.

7   In general, at all Atlantic stations (*i.e.* stations 1 to 4), the vertical distribution of $[dCu]_T$ was

8   consistent with the profiles reported elsewhere in the Atlantic sector (Jacquot and Moffett,

9   2015; Roshan and Wu, 2015), with $[dCu]_T$ increasing with depth below the surface mixed layer

10   (SML) (Fig. 6). An increase of $\delta^{65}Cu$ is observed with depth, with deep water masses carrying

11   heavier $\delta^{65}Cu$ (+0.60 ‰; NEADW, LDW; Fig. 6) than sub-superficial and intermediate water

12   masses (+0.45 ‰; SAW, NACW; Fig. 6). Little et al. (2018) report an average $\delta^{65}Cu$ of +0.66

13   ± 0.07‰ (n = 39, 1s.d.) below 200 m for stations in the South Atlantic, highlighting the

14   homogeneous composition of the deep Atlantic waters in $\delta^{65}Cu$.

15   Profiles of $[dCu]_T$ in the WMB stations (*i.e.* stations 5S, 11S, 12N, 13N, 17N) have an average

16   value of 1.64 ± 0.33 nmol kg^{-1} (n = 25; 1 s.d) below 200 m, and show no clear variations

17   between MAW, WMDW and LIW (fig. 6). The profiles and range of Cu concentrations in the

18   WMB stations are in accordance with previous Mediterranean studies by *e.g.* Boyle et al.

19   (1985), Laumond et al. (1984), Morley et al., (1997) and Yoon et al. (1999).

20   The profiles and range of $[dCu]_T$ at stations 18S and 5N are comparable to data reported by

21   Saager et al. (1993) in the Bannock basin. However, the profile of $[dCu]_T$ at station 21S

22   (comparatively Tyro basin) does not compare to Saager et al. (1993). The authors proposed

23   that the occurrence of anoxic brines in the Tyro basin may explain the large variations of $[dCu]_T$

24   observed in deep water, however station 21S does not show the presence of such a brine.

1   Copper isotope ratios range from +0.21 ‰ (station 21S; 10 m) to +0.76 ‰ (station 21S; 1249

2   m) (Table 3, Fig. 6). A number of low $\delta^{65}Cu$ values, from +0.21 ‰ to +0.37 ‰, were found

3   within the euphotic zone (0 - 200 m) at Atlantic station 4 and in the Southern Mediterranean

4   stations 5S to 21S. Profiles of $\delta^{65}Cu$ showed a significant increase at the Chl *a* maximum within

5   the Atlantic stations and Southern Mediterranean stations, with a non-systematic decrease in

6      $[dCu]_T$. Benthic variations in dCu and $\delta^{65}Cu$ were noted at stations 11S, 18S and 5N with no

7   systematic trend between the two parameters. The vertical distribution of $\delta^{65}Cu$ were

8   comparable to published profiles from Thompson et al. (2014; 2013), Takano et al. (2013;

9   2014) and Little et al. (2018), with $\delta^{65}Cu$ ranging from +0.46 ‰ to +0.99 ‰.

10   5. Discussion

11   5.1. Comparison between methods

12   In order to measure $\delta^{65}Cu$ in open seawater, several analytical challenges must be overcome.

13   Because dCu concentrations in natural seawater are generally below 1 nmol kg^{-1}, $\delta^{65}Cu$ should

14   be determined on 50 ng or less of Cu. Procedural blanks must be less than 1 to 2 ng so that

15   their contribution to the measured $\delta^{65}Cu$ values are negligible. The natural variability in Cu

16   isotope ratios is also expected to be in the per mil range, so an analytical precision of about 0.1

17   ‰ (2 s.d.) should be achieved. Another critical analytical aspect is the necessity to avoid

18   isobaric interferences and matrix effects during mass spectrometric analysis. Several

19   approaches have been recently reported for carrying out the pre-concentration steps required

20   to measure the Cu isotope ratio of dCu in seawater: 1) organic solvent extraction with

21   chloroform (Boyle et al., 2012; Thompson and Ellwood, 2014; Thompson et al., 2013); 2)

22      $Mg(OH)_2$ co-precipitation (Bermin et al., 2006; Vance et al., 2008); 3) use of a chelating resin

23   (Chelex-100 or Nobias-chelate PA-1 resins, (Bermin et al., 2006; Takano et al., 2013). We

24   found that the use of NTA-resin offers the advantage of efficiently discarding major

1   components of the seawater matrix (e.g. S, Si, Ca) as well as trace elements (e.g. Ni, Zn,), while

2   providing a great recovery for Cu in acidic seawater (Rouxel and Auro, 2010).

3   Previous studies have widely used Zn isotopes to correct for instrumental mass bias, thereby

4   allowing to report $\delta^{65}Cu$ after an internal normalization step (Archer and Vance, 2004;

5   Marechal et al., 1999; Zhu et al., 2000). This method implies that Zn and Cu isotopes are

6   fractionated in a similar manner during MC-ICPMS measurements, which is valid in most

7   cases, or could be assessed by measuring the relationships between Zn and Cu instrumental

8   mass fractionation factors over the course of the analytical session. In practice, this method is

9   also used in conjunction to the so-called standard-sample bracketing method (Takano et al.,

10   2013). It is, however, important to note that this method is prone to potential isobaric

11   interferences or matrix effects, especially considering that both Cu and Zn isotope systems

12   must be free of artifacts. In some instances, Ni has been used in place of Zn to correct for mass

13   bias (Boyle et al., 2012; Thompson and Ellwood, 2014; Thompson et al., 2013). We evaluated

14   the potential analytical artifacts and discussed the robustness of our method (sections 4.1-4.2).

15   The overall outcome is that sample-standard bracketing technique yields similar, if not better,

16   external precision compared to Zn-doping, with a 2 s.d. of about 0.06 ‰. The use of a standard-

17   sample bracketing with no external addition of Zn or Ni remains a simpler way to correct for

18   mass-bias without introducing further correction, in particular from Zn-hydride interferences,

19   which is required when measuring sample solutions with high Zn/Cu ratios (i.e, optimal

20   conditions for low Cu concentrations). The exclusive use of a spray chamber was also proven

21   to be critical to avoid potential matrix-induced artifacts in Cu isotope analysis, which cannot

22   be corrected using internal standardization using either Zn or Ni.

23   **5.2. Distribution of Cu and $\delta^{65}Cu$ in the Mediterranean Sea and Atlantic Ocean**

24   *5.2.1. Variations of Cu and $\delta^{65}Cu$ in the euphotic zone: atmospheric input.*

1   Copper concentrations and isotope ratios varied mostly within the top 200 m in the

2   Mediterranean Sea stations. Southern stations were sporadically affected by low δ^{65}Cu in sub-

3   surface and peaks in δ^{65}Cu at depth of Chl *a* maximum, while Northern stations showed more

4   constant profiles of [dCu]$_T$ and δ^{65}Cu around 1.86 ± 0.24 nmol kg^{-1} and $+0.49 \pm 0.07$‰ (1s.d.,

5   n = 14). Such variations could be linked to dCu sensitivity to aerosol deposition, river input

6   and/or biological activity, each hypothesis being discussed in the following sections 5.2.1 to

7   5.2.3 respectively.

8   Can aerosol deposition be responsible for the low δ^{65}Cu observed at stations 4, 11S, 18S, 21S

9   in surface and down to 125 m? If so, why would Northern stations not be affected by it?

10   Dissolved Cu shows a clear enrichment in surface waters along a SW-NE gradient (Fig. 7). A

11   similar pattern was reported for dAl, dFe and dCo within the same sample set, which was

12   attributed to the dissolution of aerosols in the EMB along the counter-clockwise circulation of

13   the MAW (Dulaquais et al., 2017; Gerringa et al., 2017; Rolison et al., 2015). The Hybrid

14   Single-Particle Lagrangian Integrated Trajectory (HYSPLIT) model for back trajectory

15   analysis was used to track the origin of aerosol deposition in the Northern and Southern stations

16   (see Supplement figure 1). The model showed that during sampling, the Northern stations were

17   under the influence of the highly-industrialized and populated Western Europe whereas the

18   Southern stations were under the influence of Northern Africa, *i.e.* the Saharan desert.

19   Preferential deposition of natural Saharan dust in the Southern Mediterranean Sea and

20   anthropogenic aerosol deposition in the Northern Mediterranean Sea are also reported by

21   Rossini et al. (2001).

22   The Saharan desert is a prominent source of trace metals to the oceans. Global δ^{65}Cu of the

23   soluble fraction of wet and dry atmospheric deposition is about 0.0 ‰, which is estimated from

24   a range of -0.18 ‰ to +0.3 ‰ (Dong et al., 2013; Little et al., 2014; Takano et al., 2014). Such

25   a value reflects the primary lithogenic origin of Cu in Saharan mineral dust. Aerosol deposition

1   from the Sahara would therefore be a source of isotopically lighter dCu to the upper column in

2   the Gibraltar Strait and Southern Mediterranean stations. When taking into account the

3   accumulation of atmospheric input along the MAW, the rapid mixing of the water masses in

4   the basin and the slow dissolution of natural aerosols in seawater (Mackey et al., 2014), the

5   signature of this natural aerosol input could possibly be seen down to 125 m in station 18S.

6   Equation (1) gives the fraction of $\delta^{65}Cu$ (f_{Cu}) contributed from each of the mineral dust and

7   Atlantic seawater components to the surface waters in the Southern Mediterranean Sea:

8    $$f_{Cu} = \frac{(\delta^{65}Cu_{MB} - \delta^{65}Cu_{Atl})}{(\delta^{65}Cu_{atm} - \delta^{65}Cu_{Atl})}$$

9   Using an average $\delta^{65}Cu$ for surface values in the Atlantic ($\delta^{65}Cu_{Atl} = +0.42$ ‰), an atmospheric

10   $\delta^{65}Cu$ of 0‰ ($\delta^{65}Cu_{atm}$), and all $\delta^{65}Cu$ inferior to $\delta^{65}Cu_{Atl}$ from surface to 125m at stations 4,

11   11S, 18S and 21S ($\delta^{65}Cu_{MB}$), we calculated that Saharan dust could contribute up to 50%

12   (station 21S, 10 m) to $\delta^{65}Cu$ in surface waters in the Southern Mediterranean Basins.

13   Numerous studies showed that the solubility of Cu in aerosols is superior from anthropogenic

14   sources *vs.* mineral sources (respectively 10-100 % against 1-7 %) (Desboeufs et al., 2005; Hsu

15   et al., 2005; Jordi et al., 2012; Sholkovitz et al., 2010), which could be seen in the superficial

16   enrichment in dCu in the Northern basins (Fig. 7). Aerosols of anthropogenic origin contain

17   carbon-containing particles (issued in part from fossil fuel combustion, biomass burning and

18   ship traffic), sea-salt particles and secondary organic aerosol (Arndt et al., 2017; Mallet et al.,

19   2016), as opposed to mineral phases in natural dust. Gonzalez et al. (2016) measured $\delta^{65}Cu_{AE633}$

20   from +0.04 ‰ to +0.97 ‰ (± 0.21 ‰, 2s.d.) in atmospheric particulate matter in two European

21   cities (London and Barcelona), and inferred a correlation between sources of fossil fuel

22   combustion (traffic and domestic/industrial combustion) and the heavy isotope composition of

23   the particles. As a side note, the newly certified standard ERM® AE633 is comparable to the

1   standard NIST SRM 976 (Moeller et al., 2012). The Northern stations could therefore see an

2   atmospheric input of dCu with a heavier isotope composition than the Southern stations.

3   The highest surface $[dCu]_T$ was measured at station 9N (6.00 nmol kg^{-1}), the closest to the

4   coast. High concentrations in surface waters of dCu and other trace elements (*e.g.* Zn, Mn, Co)

5   have previously been reported (Zago et al., 2002) and linked to significant atmospheric

6   deposition (Guerzoni et al., 1999; Rossini et al., 2001) and river input (Tankere and Statham,

7   1996). The sampling was done on July 31st 2013, when forest fires were detected close to the

8   location of the station (Arndt et al., 2017). Organic-rich aerosol deposits were therefore

9   expected at station 9N, and $\delta^{65}Cu$ measured in surface (+0.51 ‰) further supports the idea that

10   atmospheric deposition of non-lithogenic origin (here ashes) could carry a heavier isotope

11   composition to the surface waters than lithogenic matter from dust aerosols.

12   *5.2.2. Variations of Cu and $\delta^{65}Cu$ in the euphotic zone: river input.*

13   The inflow of surface Atlantic water across the Gibraltar Strait has been shown to bring a

14   significant pool of trace metals (*e.g.* Cu, Zn, Cd, Ni and Co) (Van Geen et al., 1988) (Fig. 7).

15   More specifically, Spanish Shelf Water (SSW) is a surface water mass that connects the Gulf

16   of Cadiz to the Gibraltar Strait during summer time, and is responsible for enriching the

17   Atlantic inflow of dCu by a factor of 2 (Elbaz-Poulichet et al., 2001). Such enrichment

18   originates within the Gulf of Cadiz, which is fed by the Rio Tinto and the Rio Odiel, two low-

19   pH rivers draining the Iberian Pyrite Belt, a massive sulfide deposit located Southern Spain and

20   Portugal (Elbaz-Poulichet et al., 1999; Nelson and Lamothe, 1993; Van Geen et al., 1997). The

21   Iberian Pyrite Belt is a historical mining site enriched in Cu sulfides (mostly chalcopyrite). In

22   a similar context, Kimball et al. (2009) measured $\delta^{65}Cu$ and [dCu] in an acidic stream, leaching

23   exposed chalcopyrite and enargite from abandoned mines in southwestern Colorado. The

24   authors found that acid leaching of Cu-enriched minerals leads to the preferential loss of ^{63}Cu

25

1 to the surface of the dissolving mineral, leaving the solution enriched in isotopically heavy

2 dCu, such as $\Delta^{65}Cu_{(solution-mineral)}$ ranges between +0.98‰ and +3.00‰ (Kimball et al., 2009;

3 Mathur et al., 2005; Wall et al., 2007).

4 Station 5S showed higher $[dCu]_T$ and heavier $\delta^{65}Cu$ in the top 60 m compared to the surface

5 waters in the Atlantic stations (Fig. 6, Table 3). In order to determine whether Cu concentration

6 and isotopic composition in surface waters at station 5S may result from mixing of Atlantic Cu

7 and Cu from the Iberian Pyrite Belt, we used the following mass balance equation (equation

8 2): $$\delta^{65}Cu_{STN\ 5S} = \delta^{65}Cu_{SSW} \times F_{SSW} + \delta^{65}Cu_{Atl.} \times F_{Atl.}$$

9 Where F is the relative contribution of the SSW and the Atlantic water masses to the surface

10 waters in the Gibraltar Strait (*i.e.* 81 ± 6% for the Atlantic water masses, and 18 ± 4% for the

11 SSW) (Elbaz-Poulichet et al., 2001), $\delta^{65}Cu_{STN\ 5S}$ is the averaged $\delta^{65}Cu$ from the top 60 m at

12 station 5S (i.e. +0.61 ±0.14‰), $\delta^{65}Cu_{Atl.}$ is the averaged $\delta^{65}Cu$ from Atlantic surface water (i.e.

13 +0.42 ±0.07‰; station 1 and BATS; this study) and $\delta^{65}Cu_{SSW}$ is the original $\delta^{65}Cu$ of SSW.

14 Modifying equation 2 to extract $\delta^{65}Cu$ from SSW at station 5S gives equation 3:

15 $$\delta^{65}Cu_{SSW} = \frac{\delta^{65}Cu_{STN\ 5S} - \delta^{65}Cu_{Atl.} \times F_{Atl.}}{F_{SSW}}$$

16 The resulting $\delta^{65}Cu$ for SSW is +1.52 ± 0.24 ‰. Measurements of $\delta^{65}Cu$ in acidic streams

17 leaching Cu sulfide minerals range from +1.38 ‰ to +1.69 ‰ (Borrok et al., 2008; Kimball et

18 al., 2009), which reinforce the validity of the calculated $\delta^{65}Cu$. However, Borrok et al. (2008)

19 measured $\delta^{65}Cu$ in freshwater upstream the Rio Tinto and Rio Odiel and found lighter values,

20 respectively -0.45 ‰ and -0.74 ‰. These values are similar to $\delta^{65}Cu$ from acid-leaching

21 experiments done on chalcopyrite in the presence of *Acidithiobacillus ferrooxidans* (dead and

22 alive) from Kimball et al. (2009). We suggest that the potential presence of such bacteria at the

23 sites of sampling may have affected the resulting $\delta^{65}Cu$ of the Rio Tinto and Rio Odiel in

24 Borrok et al. (2008), and that the reported $\delta^{65}Cu$ may not be representative of the whole rivers.

1   Finally, we cannot dismiss that heavy δ^{65}Cu measured in surface waters at station 5S may result

2   from further isotopic exchange between particulate and dissolved Cu pools downstream, as

3   previously observed in riverine systems (Vance et al., 2008). Direct measurement of δ^{65}Cu in

4   the SSW and downstream the Rio Tinto and the Rio Odiel would be necessary to confirm the

5   calculated value. However, if the similarity of the calculated δ^{65}Cu value of SSW to the Borrok

6   et al. (2008) (Fisher Creek) and Kimball et al. (2009) results is meaningful, we may suggest

7   that: (1) Cu transported by the SSW might carry the isotopic signature of Cu sulfide acidic

8   leachate, presumably originating from the Iberian Pyrite Belt; (2) the signature of Cu from the

9   Iberian Pyrite Belt may be seen as far away as the Alboran Sea.

10   For the other stations within the WMB and EMB, salinity values at all stations suggest the

11   absence of a direct influence of riverine input (Fig. 2).

12   *5.2.3. Variations of Cu and δ^{65}Cu in the euphotic zone: biological activity.*

13   The Mediterranean Sea is oligotrophic, and the Chl *a* concentrations at the Chl *a* maximum

14   varied between 0.09 and 0.67 mg m^{-3}. δ^{65}Cu showed significant increase by up to 0.5 ‰ in the

15   Chl *a* maximum in the Atlantic stations (stations 3, 4) and the Southern Mediterranean stations

16   (stations 5S, 11S, 18S and 21S). Little et al. (2018) also reported isotopically heavy dCu in the

17   Chl *a* maximum in two eutrophic stations in the South Atlantic. The authors suggested that the

18   preferential uptake of the light isotope and/or stabilization of the heavy isotope in solution

19   could lead to isotopically heavier dCu in solution.

20   The light isotope ^{63}Cu tends to adsorb onto particles or be taken up as a nutrient by

21   phytoplankton as Cu(I) (Sherman, 2013; Zhu et al., 2002). Such a loss of light isotope ^{63}Cu to

22   phytoplankton (by uptake or sinking onto particles) could therefore explain the increase in

23   δ^{65}Cu at Chl *a* maximum. Additionally, marine phytoplankton produce extracellular Cu-

24   ligands of various conditional stability constant, i.e. log K=12-14 M^{-1} for class 1-ligands, and

27

1   log K = 9-12 M^{-1} for class 2-ligands (Croot et al., 2000; Pistocchi et al., 2000; Schreiber et al.,

2   1990), resulting in the near complete organic complexation of Cu^{2+} in the dissolved pool. Ryan

3   et al. (2014) showed organic ligands preferentially complex the heavy Cu isotope in solution,

4   conferring it higher stability as dCu.

5   Interestingly, we noted that the stations presenting the lowest Chl *a* concentrations (stations

6   18S, 21S, 9N, 12N and 13N) presented the highest $\delta^{65}Cu$ average within the euphotic zone

7   (+0.54 ± 0.07 ‰, 1s.d.; n = 17) when compared to stations of higher Chl *a* content (+0.44 ±

8   0.08 ‰, 1s.d.; n = 29) (extreme values excluded). The disparity between the two averages is

9   small, but might nonetheless reflect the remineralization process at work at stations of higher

10   productivity. It is worth noting that the Mediterranean Sea stations do not show much variations

11   in $[dCu]_T$ with depth, which we believe is due to rapid mixing between intermediate and deep

12   waters and the short residence time of the water masses (Yoon et al., 1999).

13   Station 17N showed relatively high Chl *a* concentration at depth of Chl *a* maximum with no

14   variation in $\delta^{65}Cu$. Remineralisation or desorption of Cu from particulate matter with

15   consequent release of light Cu to the dissolved pool could have competed with the biological

16   activity at this station. Remineralization was reported to be limited in the Mediterranean Sea

17   (Dulaquais et al., 2017), however, we do not exclude an external source of particulate Cu (*e.g.*

18   continental run-off, coastal sediments release) as a more substantial source of isotopically light

19   dCu to the dissolved phase at this station.

20   *5.2.4. Variations of Cu and $\delta^{65}Cu$ at benthic depth.*

21   Bottom depth increases in dCu have been reported in the open Ocean and interpreted as the

22   result of the recycling of scavenged Cu during early diagenesis and supply to the overlying

23   seawater (Boyle et al., 1977; Bruland, 1980; Saager et al., 1997). At benthic depths, a

24   significant increase in $[dCu]_T$ was accompanied by concomitant decline in $\delta^{65}Cu$ at stations 3,

    28

1   11S, and 9N and 17N. A concomitant decrease in δ^{65}Cu at the sedimentary interface was also

2   observed for North Pacific and Tasmanian stations (Takano et al., 2014; Thompson et al.,

3   2013). Using a simple mixing model, we calculated for the aforementioned stations the δ^{65}Cu

4   value of the sediment source, which varied between -0.2 ‰ and +0.5 ‰ for a contribution of

5   sedimentary Cu to the dissolved pool ranging from 10 % to 50 %. Details of the equation and

6   results are available in the supplementary material as Supplementary equation 1 and

7   Supplementary table 1. The calculated range in isotopic composition of the sediment source at

8   these stations encompasses that of δ^{65}Cu in authigenic and lithogenic sediments (Little et al.,

9   2017).

10   In the Mediterranean Sea, particulate export of Cu to the sediment is mostly associated with

11   organic matter (Cossa et al., 2014; Heimbürger et al., 2014; Migon, 2005; Sakellari et al.,

12   2011), and the release of Cu by aerobic organic matter degradation into sediment pore waters

13   (Shaw et al., 1990) is likely linked to the release of isotopically-light Cu. This observation is

14   further supported by sediment-resuspension experiments, which showed that dCu in pore water

15   originates mostly from particulate organic matter degradation and that complexation of Cu with

16   dissolved organic matter in seawater stabilizes the element in solution after resuspension of the

17   sediments (Gerringa, 1990; Saulnier, 1997). The low δ^{65}Cu value of +0.33 ‰ found at 400 m

18   at station 4 could therefore be explained by sediment resuspension caused by the flow of

19   MSOW over the Gibraltar sill. In a similar way, station 5N showed a significant decrease of

20   δ^{65}Cu at 3250 m. Adriatic bottom water flows at benthic depth from the shallow Adriatic Sea

21   to the deep Ionian Sea where station 5S is located (Van Aken, 2015), and might be transporting

22   dCu released from sediment over the sharp slope of the South Adriatic Pit.

6. Conclusion

We developed and applied a new technique for the determination of δ^{65}Cu in seawater and reported variations in Cu concentration and isotope ratio for 12 stations in the Mediterranean Sea and Atlantic Ocean. The method accuracy was successfully tested through experiments and we obtained an overall analytical precision of 0.06 ‰ 2 s.d. Disparities in δ^{65}Cu between studies on GEOTRACES inter-comparison samples from the Bermuda station BATS show that there is a need for collaboration between laboratories in order to develop a new inter-comparison sample and determine how crucial the use of UV-oxidation is in dCu isotopes analysis.

Using the extensive dataset for δ^{65}Cu and [dCu]$_T$ generated in this study, we were able to observe variations mostly occurring within the euphotic zone (0 - 200 m) and at benthic depths. We suggest these variations result from a combination of addition of Cu from various sources feeding the basins, physical mixing and biological activity. Copper concentration measurements coupled with atmospheric back-tracking modeling showed a clear zonation between mineral dust deposition from the Saharan desert at the Southern Mediterranean stations *vs.* anthropogenic aerosol deposition from the populated and industrialized Western Europe at the Northern Mediterranean stations. Saharan dust deposition appears to be a source of isotopically light Cu to the Southern stations, and because dissolution rate of natural dust deposits are low, this effect appears to be seen deeper in the euphotic zone. In contrast, anthropogenic/combustion-related aerosols have a high solubility and carry δ^{65}Cu isotopically heavier than mineral dust sources, and their impact on the Northern stations appears to be at shallower depths and limited to variations in [dCu]$_T$. The possible role of the Iberian Pyrite Belt as a source of isotopically-heavy dCu to the Mediterranean Sea was also highlighted, but further study needs to address the δ^{65}Cu of dissolved and particulate phases in the Rio Tinto and Odiel rivers. We also observed a significant increase in δ^{65}Cu within the Chl a maximum

1 likely due to uptake and/or scavenging of isotopically light dCu in or onto phytoplankton.

2 Finally, at bottom depths, sediments appear to be a source of isotopically light dCu from pore

3 waters via resuspension.

4 Future studies should focus on the fractionation between dissolved, organically-complexed and

5 particulate fractions of Cu to better apprehend the processes driving Cu biogeochemical cycling

6 in seawater. A better understanding of the variations of δ^{65}Cu in seawater would allow the use

7 of δ^{65}Cu as a tool to better evaluate the origin of the missing import and export fluxes of dCu

8 in the marine realm, and the impact of anthropogenic sources on the Ocean.

20 **References**

21 Albarede, F., 2004. The stable isotope geochemistry of copper and zinc. Reviews in mineralogy
22   and geochemistry, 55(1): 406-427.
23 Ambar, I., Howe, M.R., 1979. Observations of the Mediterranean outflow .2. Deep circulation
24   in the vicinity of the Gulf of Cadiz. Deep-Sea Research Part a-Oceanographic Research
25   Papers, 26(5): 555-568.
26 Archer, C., Vance, D., 2004. Mass discrimination correction in multiple-collector plasma
27   source mass spectrometry: an example using Cu and Zn isotopes. Journal of Analytical
28   Atomic Spectrometry, 19(5): 656-665.

Arndt, J. et al., 2017. Sources and mixing state of summertime background aerosol in the north-western Mediterranean basin. Atmospheric Chemistry and Physics, 17(11): 6975-7001.

Babcsanyi, I. et al., 2016. Copper in soil fractions and runoff in a vineyard catchment: Insights from copper stable isotopes. Science of the Total Environment, 557: 154-162.

Babcsanyi, I., Imfeld, G., Granet, M., Chabaux, F., 2014. Copper Stable Isotopes To Trace Copper Behavior in Wetland Systems. Environmental Science & Technology, 48(10): 5520-5529.

Bermin, J., Vance, D., Archer, C., Statham, P.J., 2006. The determination of the isotopic composition of Cu and Zn in seawater. Chemical Geology, 226(3-4): 280-297.

Bethoux, J.P., 1980. Mean water fluxes across sections in the Mediterranean-Sea, evaluated on the basis of water and salt budgets and of observed salinities. Oceanologica Acta, 3(1): 79-88.

Bigalke, M., Weyer, S., Wilcke, W., 2010. Copper Isotope Fractionation during Complexation with Insolubilized Humic Acid. Environmental Science & Technology, 44(14): 5496-5502.

Bigalke, M., Weyer, S., Wilcke, W., 2011. Stable Cu isotope fractionation in soils during oxic weathering and podzolization. Geochimica Et Cosmochimica Acta, 75(11): 3119-3134.

Biller, D.V., Bruland, K.W., 2012. Analysis of Mn, Fe, Co, Ni, Cu, Zn, Cd, and Pb in seawater using the Nobias-chelate PA1 resin and magnetic sector inductively coupled plasma mass spectrometry (ICP-MS). Marine Chemistry, 130: 12-20.

Borrok, D.M., Nimick, D.A., Wanty, R.B., Ridley, W.I., 2008. Isotopic variations of dissolved copper and zinc in stream waters affected by historical mining. Geochimica et Cosmochimica Acta, 72(2): 329-344.

Borrok, D.M. et al., 2007. Separation of copper, iron, and zinc from complex aqueous solutions for isotopic measurement. Chemical Geology, 242(3-4): 400-414.

Boyle, E.A., Chapnick, S.D., Bai, X.X., Spivack, A., 1985. Trace-metal enrichments in the Mediterranean-Sea. Earth and Planetary Science Letters, 74(4): 405-419.

Boyle, E.A. et al., 2012. GEOTRACES IC1 (BATS) contamination-prone trace element isotopes Cd, Fe, Pb, Zn, Cu, and Mo intercalibration. Limnology and Oceanography-Methods, 10: 653-665.

Boyle, E.A., Sclater, F.R., Edmond, J.M., 1977. The distribution of dissolved copper in the Pacific. Earth and Planetary Science Letters, 37(1): 38-54.

Bruland, K.W., 1980. Oceanographic distributions of cadmium, zinc, nickel, and copper in the North Pacific. Earth and Planetary Science Letters, 47(2): 176-198.

Bruland, K.W., Franks, R.P., 1983. Mn, Ni, Cu, Zn and Cd in the Western North Atlantic, Trace Metals in Sea Water. NATO Conference Series. Springer US, pp. 395-414.

Coale, K.H., Bruland, K.W., 1988. Copper complexation in the Northeast Pacific. Limnology and Oceanography, 33(5): 1084-1101.

Coale, K.H. et al., 1996. A massive phytoplankton bloom induced by an ecosystem-scale iron fertilization experiment in the equatorial Pacific Ocean. Nature, 383(6600): 495-501.

Cossa, D. et al., 2014. Origin and accumulation of trace elements in sediments of the northwestern Mediterranean margin. Chemical Geology, 380: 61-73.

Coste, B., Lecorre, P., Minas, H.J., 1988. Reevaluation of the nutrient exchanges in the Strait of Gibraltar. Deep-Sea Research Part a-Oceanographic Research Papers, 35(5): 767-775.

Croot, P.L., Moffett, J.W., Brand, L.E., 2000. Production of extracellular Cu complexing ligands by eucaryotic phytoplankton in response to Cu stress. Limnology and Oceanography, 45(3): 619-627.

Cutter, C. et al., 2014. Sampling and Sample-handling Protocols for GEOTRACES Cruises (version 2.0). In: www.geotraces.org/ (Editor).

De Baar, H.J.W. et al., 2008. Titan: A new facility for ultraclean sampling of trace elements and isotopes in the deep oceans in the international Geotraces program. Marine Chemistry, 111(1-2): 4-21.

Desboeufs, K.V., Sofikitis, A., Losno, R., Colin, J.L., Ausset, P., 2005. Dissolution and solubility of trace metals from natural and anthropogenic aerosol particulate matter. Chemosphere, 58(2): 195-203.

Dong, S.F. et al., 2013. Stable isotope ratio measurements of Cu and Zn in mineral dust (bulk and size fractions) from the Taklimakan Desert and the Sahel and in aerosols from the eastern tropical North Atlantic Ocean. Talanta, 114: 103-109.

Duce, R.A., Tindale, N.W., 1991. Atmospheric transport of Iron and its deposition in the ocean. Limnology and Oceanography, 36(8): 1715-1726.

Dulaquais, G., Planquette, H., L'Helguen, S., Rijkenberg, M.J.A., Boye, M., 2017. The biogeochemistry of cobalt in the Mediterranean Sea. Global Biogeochemical Cycles, 31(2): 377-399.

Ehrlich, S. et al., 2004. Experimental study of the copper isotope fractionation between aqueous Cu(II) and covellite, CuS. Chemical Geology, 209: 259– 269.

Elbaz-Poulichet, F., Morley, N.H., Beckers, J.M., Nomerange, P., 2001. Metal fluxes through the Strait of Gibraltar: the influence of the Tinto and Odiel rivers (SW Spain). Marine Chemistry, 73(3-4): 193-213.

Elbaz-Poulichet, F. et al., 1999. Trace metal and nutrient distribution in an extremely low pH(2.5) river-estuarine system, the Ria of Huelva (South-West Spain). Science of the Total Environment, 227(1): 73-83.

Fujii, T., Moynier, F., Abe, M., Nemoto, K., Albarède, F., 2013. Copper isotope fractionation between aqueous compounds relevant to low temperature geochemistry and biology. Geochimica et Cosmochimica Acta, 110: 29–44.

Gascard, J.C., Richez, C., 1985. Water masses and circulation in the Western Alboran Sea and in the Straits of Gibraltar. Progress in Oceanography, 15(3): 157-216.

Gerringa, L.J.A., 1990. Aerobic degradation of organic matter and the mobility of Cu, Cd, Ni, Pb, Zn, Fe and Mn in marine sediment slurries. Marine Chemistry, 29(4): 355-374.

Gerringa, L.J.A. et al., 2017. Dissolved Fe and Fe -binding organic ligands in the Mediterranean Sea GEOTRACES G04. Marine Chemistry, 194: 100-113.

Gonzalez, R.O. et al., 2016. New Insights from Zinc and Copper Isotopic Compositions into the Sources of Atmospheric Particulate Matter from Two Major European Cities. Environmental Science and Technology, 50(18): 9816-9824.

Goudie, A.S., Middleton, N.J., 2001. Saharan dust storms: nature and consequences. Earth-Science Reviews, 56(1-4): 179-204.

Graham, S., Pearson, N., Jackson, S., Griffin, W., O'reilly, S.Y., 2004. Tracing Cu and Fe from source to porphyry: in situ determination of Cu and Fe isotope ratios in sulfides from the Grasberg Cu–Au deposit. Chemical Geology, 207(3-4): 147-169.

Guerzoni, S. et al., 1999. The role of atmospheric deposition in the biogeochemistry of the Mediterranean Sea. Progress in Oceanography, 44(Issues 1–3): 147–190.

Guieu, C., Martin, J.M., Thomas, A.J., Elbazpoulichet, F., 1991. Atmospheric versus river inputs of metals to the Gulf of Lions - Total concentrations, partitioning and fluxes. Marine Pollution Bulletin, 22(4): 176-183.

Heimbürger, L.E. et al., 2014. Vertical export flux of metals in the Mediterranean Sea. Deep Sea Research Part I: Oceanographic Research Papers, 87: 14–23.

Herut, B. et al., 2005. Response of East Mediterranean surface water to Saharan dust: On-board microcosm experiment and field observations. Deep-Sea Research Part II-Topical Studies in Oceanography, 52(22-23): 3024-3040.

Howe, M.R., 1982. The Mediterranean water outflow in the Gulf of Cadiz. Oceanography and Marine Biology, 20: 37-64.

Hsu, S.C., Lin, F.J., Jeng, W.L., 2005. Seawater solubility of natural and anthropogenic metals within ambient aerosols collected from Taiwan coastal sites. Atmospheric Environment, 39(22): 3989-4001.

Jacquot, J.E., Moffett, J.W., 2015. Copper distribution and speciation across the International GEOTRACES Section GA03. Deep Sea Research Part II: Topical Studies in Oceanography, 116: 187-207.

Jordi, A., Basterretxea, G., Tovar-Sanchez, A., Alastuey, A., Querol, X., 2012. Copper aerosols inhibit phytoplankton growth in the Mediterranean Sea. Proceedings of the National Academy of Sciences of the United States of America, 109(52): 21246-21249.

Kimball, B.E. et al., 2009. Copper isotope fractionation in acid mine drainage. Geochimica Et Cosmochimica Acta, 73(5): 1247-1263.

Larson, P.B. et al., 2003. Copper isotope ratios in magmatic and hydrothermal ore-forming environments. Chemical Geology, 201(3-4): 337-350.

Laubier, L., 2005. Mediterranean Sea and Humans: improving a conflictual partnership. In: Saliot, A. (Ed.), The Mediterranean Sea. The Handbook of Environmental Chemistry. Springer-Verlag Berlin Heidelberg, pp. 3-27.

Laumond, F., Copinmontegut, G., Courau, P., Nicolas, E., 1984. Cadmium, copper and lead in the Western Mediterranean Sea. Marine Chemistry, 15(3): 251-261.

Little, S.H. et al., 2018. Paired dissolved and particulate phase Cu isotope distributions in the South Atlantic. Chemical Geology.

Little, S.H., Vance, D., McManus, J., Severmann, S., Lyons, T.W., 2017. Copper isotope signatures in modern marine sediments. Geochimica Et Cosmochimica Acta, 212: 253-273.

Little, S.H., Vance, D., Siddall, M., Gasson, E., 2013. A modeling assessment of the role of reversible scavenging in controlling oceanic dissolved Cu and Zn distributions. Global Biogeochemical Cycles, 27(3): 780-791.

Little, S.H., Vance, D., Walker-brown, C., Landing, W.M., 2014. The oceanic mass balance of copper and zinc isotopes, investigated by analysis of their inputs, and outputs to ferromanganese oxide sediments. Geochimica et Cosmochimica Acta(125): 673-693.

Lohan, M.C., Aguilar-Islas, A.M., Franks, R.P., Bruland, K.W., 2005. Determination of iron and copper in seawater at pH 1.7 with a new commercially available chelating resin, NTA Superflow. Analytica Chimica Acta, 530(1): 121–129.

Ludwig, W., Dumont, E., Meybeck, M., Heussner, S., 2009. River discharges of water and nutrients to the Mediterranean and Black Sea: Major drivers for ecosystem changes during past and future decades? Progress in Oceanography, 80(3-4): 199-217.

Mackey, K.R.M., Chien, C.T., Post, A.F., Saito, M.A., Paytan, A., 2014. Rapid and gradual modes of aerosol trace metal dissolution in seawater. Frontiers in Microbiology, 5(794).

Maher, K.C., Larson, P.B., 2007. Variation in Copper Isotope Ratios and Controls on Fractionation in Hypogene Skarn Mineralization at Coroccohuayco and Tintaya, Perú. Economic Geology, 102: 225-237.

Mallet, M. et al., 2016. Overview of the Chemistry-Aerosol Mediterranean Experiment/Aerosol Direct Radiative Forcing on the Mediterranean Climate (ChArMEx/ADRIMED) summer 2013 campaign. Atmospheric Chemistry and Physics, 16(2): 455-504.

Marechal, C.N., Telouk, P., Albarede, F., 1999. Precise analysis of copper and zinc isotopic compositions by plasma-source mass spectrometry. Chemical Geology, 156(1-4): 251-273.

Mariotti, A., Struglia, M.V., Zeng, N., Lau, K.M., 2002. The hydrological cycle in the Mediterranean region and implications for the water budget of the Mediterranean Sea. Journal of Climate, 15(13): 1674-1690.

Mason, T.F.D. et al., 2005. Zn and Cu isotopic variability in the Alexandrinka volcanic-hosted massive sulphide (VHMS) ore deposit, Urals, Russia. Chemical Geology, 221: 170-187.

Mason, T.F.D. et al., 2004. High-precision Cu and Zn isotope analysis by plasma source mass spectrometry - Part 1. Spectral interferences and their correction. Journal of Analytical Atomic Spectrometry, 19(2): 209-217.

Mathur, R. et al., 2005. Cu isotopic fractionation in the supergene environment with and without bacteria. Geochimica et Cosmochimica Acta, 69: 5233–5246.

May, T.W., Wiedmeyer, R.H., 1998. A table of polyatomic interferences in ICP-MS. Atomic Spectroscopy, 19(5): 150-155.

McDougall, T.J., Barker, P.M., 2011. Getting started with the TEOS-10 and the Gibbs Seawater (GSW) Oceanographic Toolbox. In: WG127, S.I. (Editor).

Middag, R. et al., 2015. Intercomparison of dissolved trace elements at the Bermuda Atlantic Time Series station. Marine Chemistry, 177(3): 476-489.

Migon, C., 2005. Trace metals in the Mediterranean Sea. In: Saliot, A. (Ed.), The Mediterranean Sea. The Handbook of environmental chemistry. Berlin-Heidelberg Springer-Verlag, pp. 151-176.

Millot, C., Taupier-Letage, I., 2005. Circulation in the Mediterranean sea. In: Saliot, A. (Ed.), The Mediterranean Sea. The Handbook of Environmental Chemistry. Springer Verlag Berlin-Heidelberg, pp. 29-66.

Milne, A., Landing, W., Bizimis, M., Morton, P., 2010. Determination of Mn, Fe, Co, Ni, Cu, Zn, Cd and Pb in seawater using high resolution magnetic sector inductively coupled mass spectrometry (HR-ICP-MS). Analytica Chimica Acta, 665(2): 200-207.

Moeller, K., Schoenberg, R., Pedersen, R.-B., Weiss, D., Dong, S., 2012. Calibration of the New Certified Reference Materials ERM-AE633 and ERM-AE647 for Copper and IRMM-3702 for Zinc Isotope Amount Ratio Determinations. Geostandards and Geoanalytical Research, 36(2): 177-199.

Moffett, J.W., Brand, L.E., 1996. Production of strong, extracellular Cu chelators by marine cyanobacteria in response to Cu stress. Limnology and Oceanography, 41(3): 388-395.

Moffett, J.W., Brand, L.E., Croot, P.L., Barbeau, K.A., 1997. Cu speciation and cyanobacterial distribution in harbors subject to anthropogenic Cu inputs. Limnology and Oceanography, 42(5): 789-799.

Moffett, J.W., Dupont, C., 2007. Cu complexation by organic ligands in the sub-arctic NW Pacific and Bering Sea. Deep-Sea Research Part I-Oceanographic Research Papers, 54(4): 586-595.

Moffett, J.W., Zika, R.G., Brand, L.E., 1990. Distribution and potential sources and sinks of copper chelators in the Sargasso Sea. Deep-Sea Research Part a-Oceanographic Research Papers, 37(1): 27-36.

Morley, N.H., Burton, J.D., Tankere, S.P.C., Martin, J.M., 1997. Distribution and behaviour of some dissolved trace metals in the western Mediterranean Sea. Deep-Sea Research Part II-Topical Studies in Oceanography, 44(3-4): 675-691.

Moynier, F., Vance, D., Fujii, T., Savage, P., 2017. The Isotope Geochemistry of Zinc and Copper. In: Teng, F.Z., Watkins, J., Dauphas, N. (Eds.), Non-Traditional Stable Isotopes. Reviews in Mineralogy & Geochemistry. Mineralogical Society of America & Geochemical Society, Chantilly, pp. 543-600.

Navarrete, J.U., Borrok, D.M., Viveros, M., Ellzey, J.T., 2011. Copper isotope fractionation during surface adsorption and intracellular incorporation by bacteria. Geochimica Et Cosmochimica Acta, 75(3): 784-799.

Nelson, C.H., Lamothe, P.J., 1993. Heavy-metal anomalies in the Tinto and Odiel river and estuary system, Spain. Estuaries, 16(3A): 496-511.

Peers, G., Price, N.M., 2006. Copper-containing plastocyanin used for electron transport by an oceanic diatom. Nature, 441(7091): 341-344.

Peers, G., Quesnel, S.A., Price, N.M., 2005. Copper requirements for iron acquisition and growth of coastal and oceanic diatoms. Limnology and Oceanography, 50(4): 1149-1158.

Pistocchi, R., Mormile, M.A., Guerrini, F., Isani, G., Boni, L., 2000. Increased production of extra- and intracellular metal-ligands in phytoplankton exposed to copper and cadmium | SpringerLink. Journal of Applied Phycology, 12(3-5): 469-477.

Pokrovsky, O.S., Viers, J., Emnova, E.E., Kompantseva, E.I., Freydier, R., 2008. Copper isotope fractionation during its interaction with soil and aquatic microorganisms and metal oxy(hydr)oxides: Possible structural control. Geochimica et Cosmochimica Acta, 72: 1742-1757.

Posacka, A.M. et al., 2017. Dissolved copper (dCu) biogeochemical cycling in the subarctic Northeast Pacific and a call for improving methodologies. Marine Chemistry(196): 47-61.

Richardson, P.L., Bower, A.S., Zenk, W., 2000. A census of Meddies tracked by floats. Progress in Oceanography, 45(2): 209-250.

Rijkenberg, M.J.A., 2013a. MedBlack GEOTRACES leg 1, cruise report 64PE370 on RV Pelagia, 14 May - 5 June 2013.

Rijkenberg, M.J.A., 2013b. MedBlack GEOTRACES leg 3, cruise report 64PE374 on RV Pelagia, 25 July - 11 August 2013.

Robinson, A.R., Leslie, W.G., Theocharis, A., Lascaratos, A., 2001. Mediterranean sea circulation. In: Steele, J.H., Thorpe , S.A., Turekian, K.K. (Eds.), Ocean currents: a derivative of the Encyclopedia of Ocean Sciences. Academic Press, pp. 1689-1705.

Robinson, A.R. et al., 1992. General circulation of the Eastern Mediterranean. Earth-Science Reviews, 32(4): 285-309.

Rolison, J.M., Middag, R., Stirling, C.H., Rijkenberg, M.J.A., de Baar, H.J.W., 2015. Zonal distribution of dissolved aluminium in the Mediterranean Sea. Marine Chemistry, 177: 87-100.

Rolph, G., Stein, A., Stunder, B., 2015. Real-time Environmental Applications and Display sYstem: READY. Environmental Modelling & Software, 95: 210-228.

Roshan, S., Wu, J.F., 2015. The distribution of dissolved copper in the tropical-subtropical north Atlantic across the GEOTRACES GA03 transect. Marine Chemistry, 176: 189-198.

Rossini, P. et al., 2001. Atmospheric deposition of trace metals in North Adriatic Sea, Mediterranean Ecosystems: Structures and Processes. Springer, Milano, pp. 123-129.

Rouxel, O., Fouquet, Y., Ludden, J.N., 2004. Copper Isotope systematics of the Lucky Strike, Rainbow and Logatchev Seafloor Hydrothermal Fields on the Mid Atlantic Ridge. Econ. Geol., 99: 585-600.

Rouxel, O.J., Auro, M., 2010. Iron Isotope Variations in Coastal Seawater Determined by Multicollector ICP-MS. Geostandards and Geoanalytical Research, 34(2): 135-144.

Rue, E., Bruland, K., 2001. Domoic acid binds iron and copper: a possible role for the toxin produced by the marine diatom Pseudo-nitzschia. Marine Chemistry, 76(1-2): 127-134.

1   Ryan, B.M., Kirby, J.K., Degryse, F., Scheiderich, K., McLaughlin, M.J., 2014. Copper Isotope
2   Fractionation during Equilibration with Natural and Synthetic Ligands. Environmental
3   Science & Technology, 48(15): 8620-8626.
4   Saager, P.M., De Baar, H.J.W., R.J., H., 1992. Cd, Zn, Ni and Cu in the Indian Ocean. Deep
5   Sea Research Part A. Oceanographic Research Papers, 39(1): 9-35.
6   Saager, P.M., deBaar, H.J.W., deJong, J.T.M., Nolting, R.F., Schijf, J., 1997. Hydrography and
7   local sources of dissolved trace metals Mn, Ni, Cu, and Cd in the northeast Atlantic
8   Ocean. Marine Chemistry, 57(3-4): 195-216.
9   Saager, P.M., Schijf, J., De Baar, H.J.W., 1993. Trace-metal distributions in seawater and
10   anoxic brines in the Eastern Mediterranean Sea. Geochimica et Cosmochimica Acta,
11   57(7): 1419-1432.
12   Sakellari, A., Plavsic, M., Karavoltsos, S., Dassenakis, M., Scoullos, M., 2011. Assessment of
13   copper, cadmium and zinc remobilization in Mediterranean marine coastal sediments.
14   Estuarine Coastal and Shelf Science, 91(1): 1-12.
15   Saulnier, I., 1997. Trace metal remobilization following the resuspension of Saguenay Fjord
16   sediments, McGill University, Montreal, Quebec, Canada.
17   Schlitzer, R., 2016. Ocean Data View, http://odv.awi.de.
18   Schreiber, D.R., Millero, F.J., Gordon, A.S., 1990. Production of an extracellular copper-
19   binding compound by the heterotrophic marine bacterium Vibrio alginolyticus. Marine
20   Chemistry, 28(4): 275-284.
21   Semeniuk, D.M., Bundy, R.M., Payne, C.D., Barbeau, K.A., Maldonado, M.T., 2015.
22   Acquisition of organically complexed copper by marine phytoplankton and bacteria in
23   the northeast subarctic Pacific Ocean. Marine Chemistry, 173: 222-233.
24   Semeniuk, D.M. et al., 2009. Plankton copper requirements and uptake in the subarctic
25   Northeast Pacific Ocean. Deep Sea Research Part I: Oceanographic Research Papers,
26   56(7): 1130-1142.
27   Send, U. et al., 1999. Recent advances in observing the physical oceanography of the western
28   Mediterranean Sea. Progress in Oceanography, 44(1-3): 37-64.
29   Shaw, T.J., Gieskes, J.M., Jahnke, R.A., 1990. Early diagenesis in differing depositional
30   environments - The response of transition metals in pore water. Geochimica Et
31   Cosmochimica Acta, 54(5): 1233-1246.
32   Sherman, D.M., 2013. Equilibrium isotopic fractionation of copper during oxidation/reduction,
33   aqueous complexation and ore-forming processes: Predictions from hybrid density
34   functional theory. Geochimica Et Cosmochimica Acta, 118: 85-97.
35   Sholkovitz, E.R., Sedwick, P.N., Church, T.M., 2010. On the fractional solubility of copper in
36   marine aerosols: Toxicity of aeolian copper revisited. Geophysical Research Letters,
37   37: 4.
38   Stein, A.F. et al., 2015. NOAA's HYSPLIT atmospheric transport and dispersion modeling
39   system. Bulletin of American Meteorological Society, 96: 2059-2077.
40   Takano, S., Tanimizu, M., Hirata, T., Sohrin, Y., 2013. Determination of isotopic composition
41   of dissolved copper in seawater by multi-collector inductively coupled plasma mass
42   spectrometry after pre-concentration using an ethylenediaminetriacetic acid chelating
43   resin. Analytica chimica acta, 784.
44   Takano, S., Tanimizu, M., Hirata, T., Sohrin, Y., 2014. Isotopic constraints on biogeochemical
45   cycling of copper in the ocean. Nature Communications, 5: 7.
46   Tankere, S.P.C., Statham, P.J., 1996. Distribution of dissolved Cd, Cu, Ni and Zn in the
47   Adriatic Sea. Marine Pollution Bulletin, 32(8-9): 623-630.
48   Ternon, E., Guieu, C., Ridame, C., L'Helguen, S., Catala, P., 2011. Longitudinal variability of
49   the biogeochemical role of Mediterranean aerosols in the Mediterranean Sea.
50   Biogeosciences, 8(5): 1067-1080.

Thompson, C.M., Ellwood, M.J., 2014. Dissolved copper isotope biogeochemistry in the Tasman Sea, SW Pacific Ocean. Marine Chemistry, 165: 1-9.

Thompson, C.M., Ellwood, M.J., Wille, M., 2013. A solvent extraction technique for the isotopic measurement of dissolved copper in seawater. Analytica Chimica Acta, 775: 106-113.

Van Aken, H.M., 2015. The hydrography encountered during the GEOTRACES/MedBlack programme (2013).

Van Geen, A., Adkins, J.F., Boyle, E.A., Nelson, C.H., Palanques, A., 1997. A 120-yr record of widespread contamination from mining of the Iberian pyrite belt. Geology, 25.

Van Geen, A., Boyle, E., 1990. Variability of trace-metal fluxes through the Strait of Gibraltar. Palaeogeography, Palaeoclimatology, Palaeoecology, 89: 65-75.

Van Geen, A., Rosener, P., Boyle, E., 1988. Entrainment of trace-metal-enriched Atlantic-shelf water in the inflow to the Mediterranean-Sea. Nature, 331(6155): 423-426.

Van Geen, A.F.M.J., 1989. Trace metal sources for the Atlantic inflow to the Mediterranean Sea. Thesis Thesis, Massachusetts Institute of Technology, Massachussetts Institute of Technology, 179 pp.

Vance, D. et al., 2008. The copper isotope geochemistry of rivers and the oceans. Earth and Planetary Science Letters, 274: 204-213.

Wall, A.J., Heaney, P.J., Mathur, R., Post, J.E., 2007. Insights into copper isotope fractionation during the oxidative phase transition of chalcocite, using time-resolved synchrotron X-ray diffraction. Geochimica Et Cosmochimica Acta, 71(15): A1081-A1081.

Yoon, Y.-Y., Martin, J.-M., Cottéc, M.H., 1999. Dissolved trace metals in the Western Mediterranean Sea: total concentration and fraction isolated by C18 Sep-Pak technique. Marine Chemistry, 66(Issues 3–4): 129–148.

Zago, C. et al., 2002. Heavy metal distribution and speciation in the Northern Adriatic Sea. Chemistry and Ecology, 18(1-2): 39-51.

Zenk, W., Armi, L., 1990. The complex spreading pattern of Mediterranean water off the Portuguese continental-slope. Deep-Sea Research Part a-Oceanographic Research Papers, 37(12): 1805-1823.

Zhu, X.K. et al., 2002. Mass fractionation processes of transition metal isotopes. Earth Planet. Sci. Lett., 200: 47-62.

Zhu, X.K., O'Nions, R.K., Guo, Y., Belshaw, N.S., Rickard, D., 2000. Determination of natural Cu-isotope variation by plasma-source mass spectrometry: implications for use as geochemical tracers. Chemical Geology, 163(1-4): 139-149.

Zumft, W.G., Kroneck, P.M.H., 2007. Respiratory transformation of nitrous oxide (N(2)O) to dinitrogen by Bacteria and Archaea. In: Poole, R.K. (Ed.), Advances in Microbial Physiology, Vol 52. Advances in Microbial Physiology. Academic Press Ltd-Elsevier Science Ltd, London, pp. 107-+.

1 Figures and Figure captions
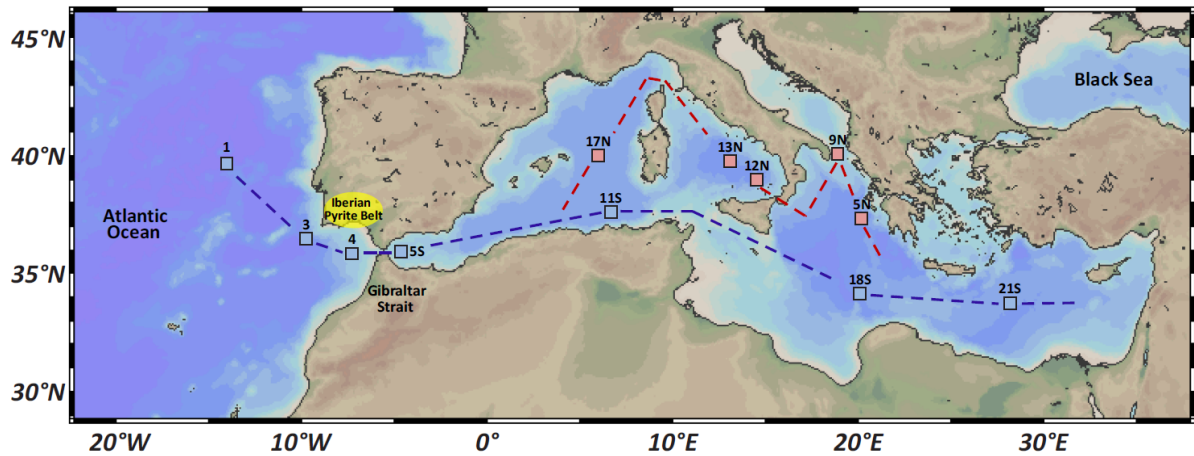
Figure 1: Location of the seawater stations sampled in the Mediterranean Sea and Atlantic Ocean. The blue dashed line represents part of the southern route of the cruise, going from Atlantic to South-East Mediterranean Sea. The red dashed line represents portion of the northern route, going from North-East Mediterranean Sea to North-West Mediterranean Sea.
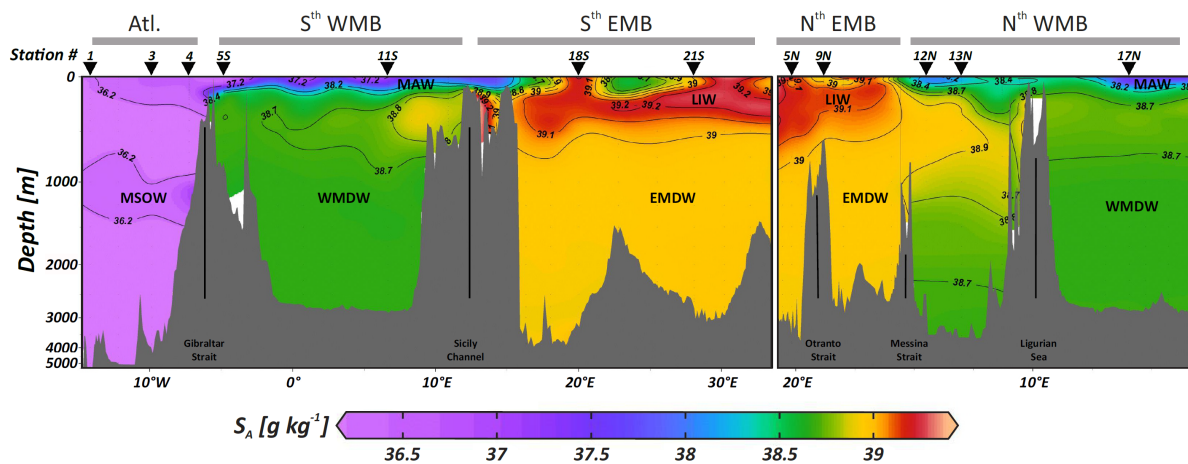
Figure 2: Absolute salinity (S_A) along the transects shown in Fig. 1. Water masses are labelled as: MAW (Modified Atlantic Water), MSOW (Mediterranean Sea Outflow Water), WMDW (Western Deep Mediterranean Water), EMDW (Eastern Mediterranean Deep Water), LIW (Levantine Intermediate Water).
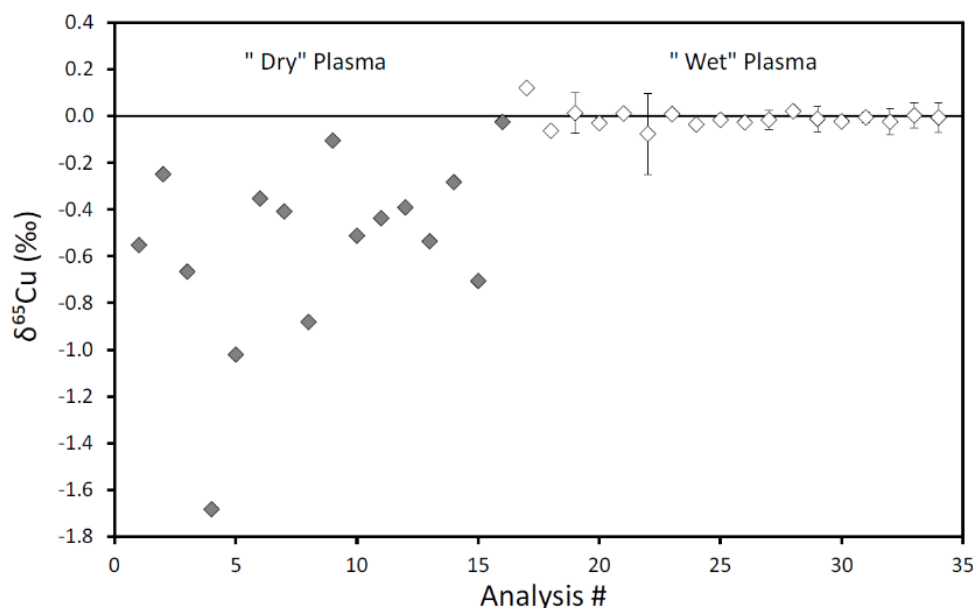
1 Figure 3: Corrected data on ultra-pure water enriched in standard Cu SRM976 after chemistry.
2 Two types of introduction systems were used for the analysis: a desolvating nebulizer Apex-Q
3 (grey diamonds) and a cyclonic spray chamber (white diamonds). Most of the samples were
4 analyzed once. The samples analyzed several times are reported with an error bar at 2 s.d.
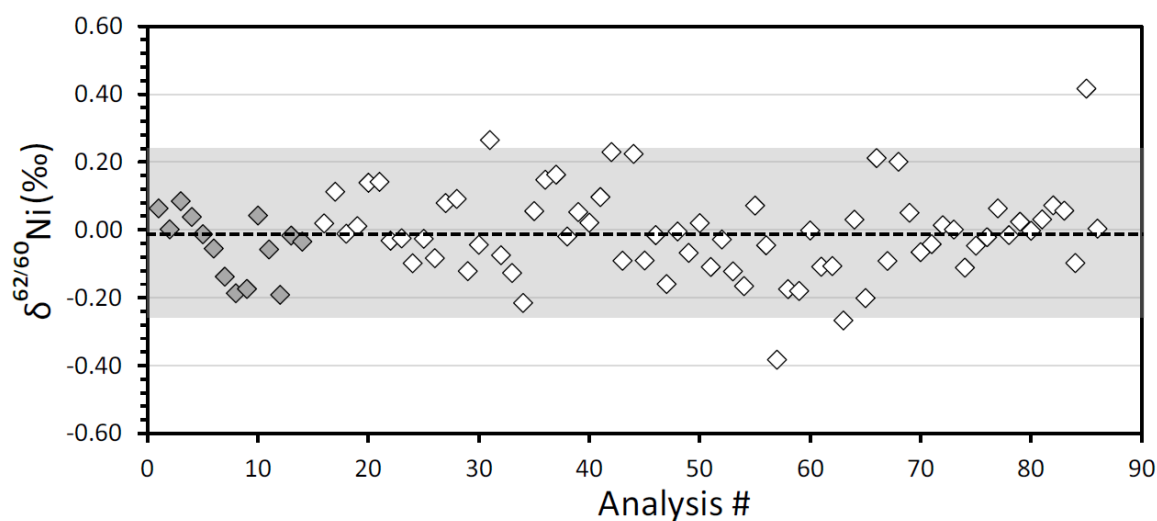
5 Figure 4: $\delta^{62/60}$Ni data on ultra-pure water enriched in standard Cu SRM976 (5 to 15 ng ml^{-1})
6 and Ni SRM3136 (50 to 100 ng ml^{-1}) after chemistry (grey diamonds), and standard solution
7 of Cu SRM976 (10 to 20 ng ml^{-1}) and Ni SRM3136 (50 to 100 ng ml^{-1}) used as inter-calibrating
8 standards during the analysis (white diamonds). The average $\delta^{62/60}$Ni value for both standards
9 and spiked blanks is -0.01 ± 0.25 ‰ (2s.d.; n = 85). Both desolvating nebulizer Apex-Q and
10 cyclonic spray chambers were used as introduction system and the analysis was done at
11 medium resolution.
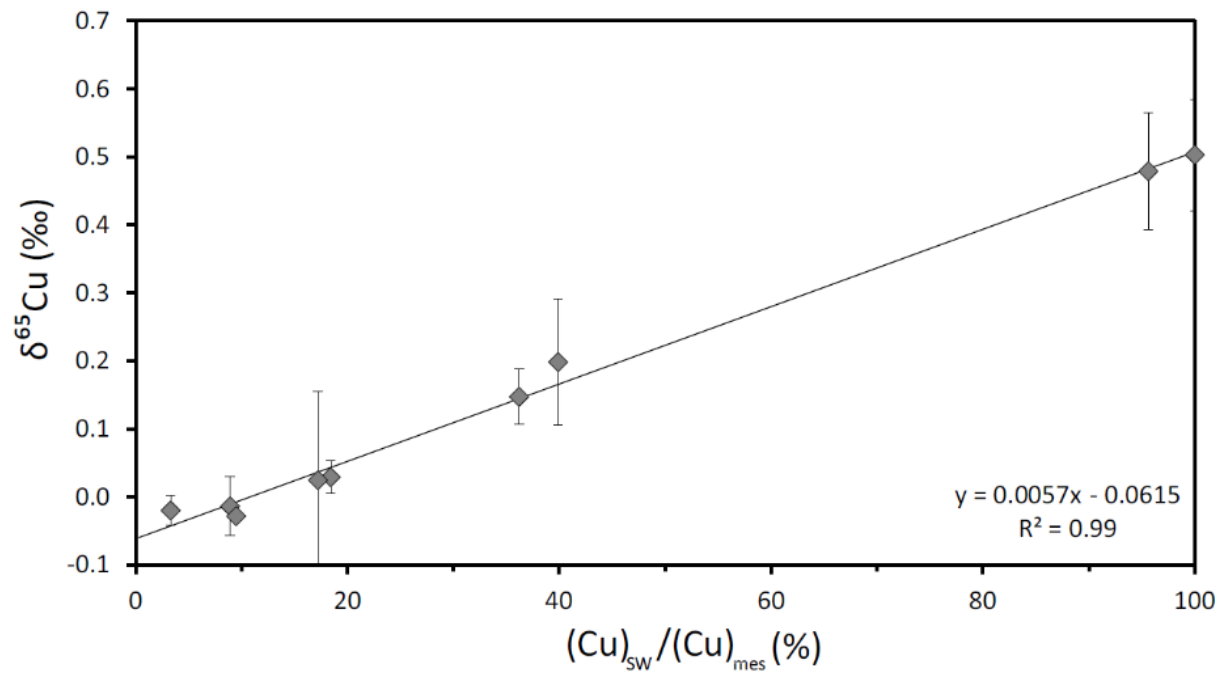
Figure 5: δ^{65}Cu measured for a bulk of seawater over the ratio natural Cu/standard Cu SRM3114 added at various amount.

1 Figure 6: Depth profiles of [dCu]$_T$ (nmol kg^{-1}, white diamonds) and δ^{65}Cu (‰ SRM976, grey diamonds) for all stations (besides station 1) in the
2 Atlantic section, North and South Western Mediterranean Basin (NWMB and SWMB), North and south Eastern Mediterranean Basin (NEMB and
3 SEMB), with approximate location of the water masses (see text for abbreviations), surface mixed layer (SML) and the depth of the Chl *a* max.
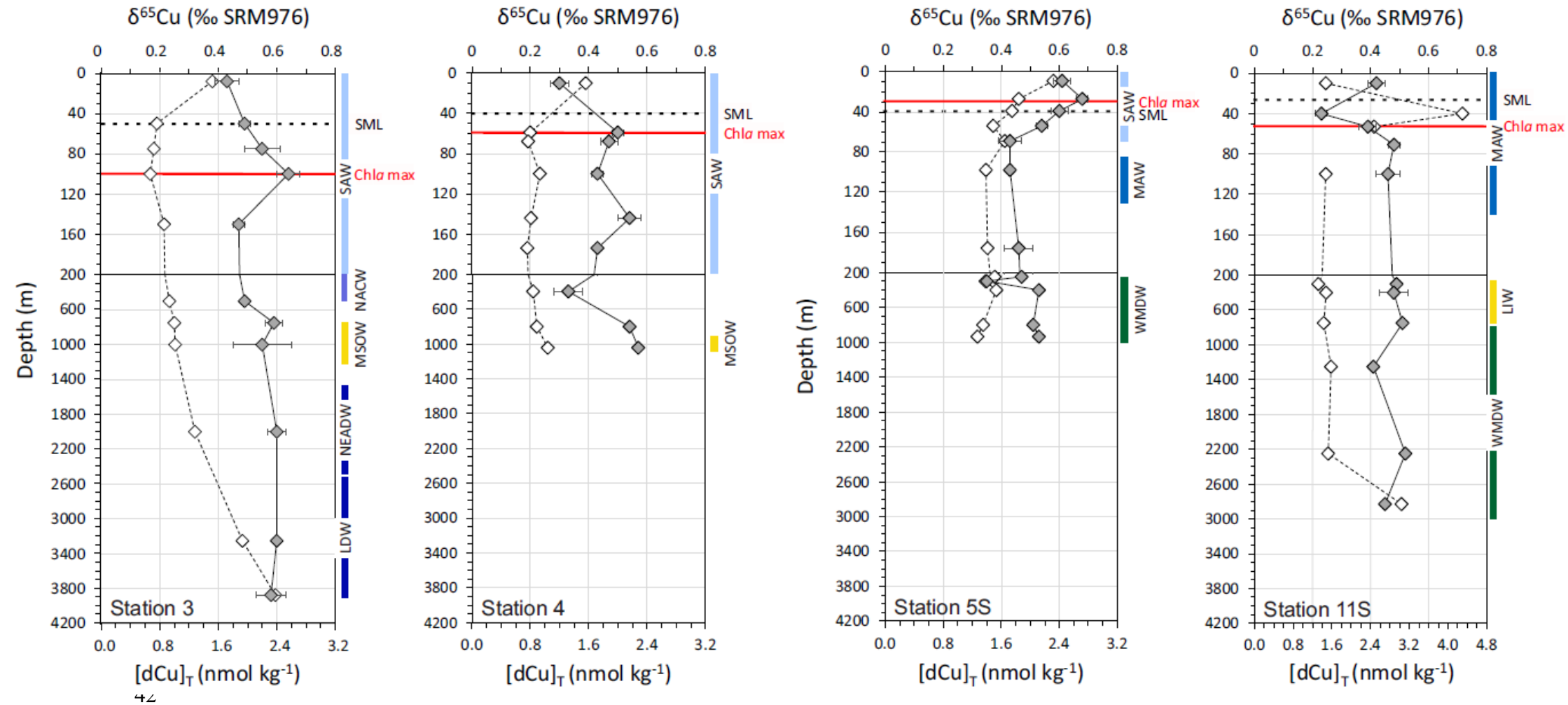
1   Figure 6: continued.
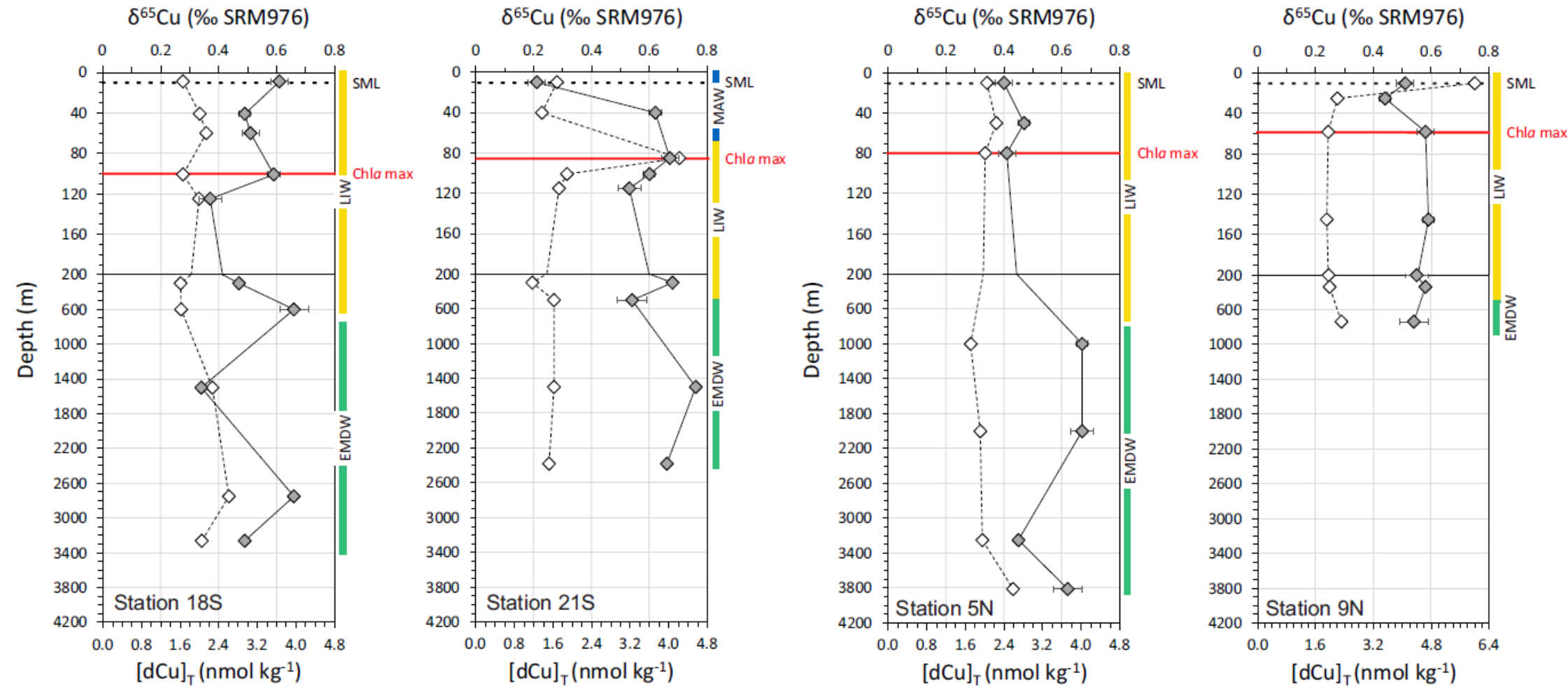
1   Figure 6: continued.
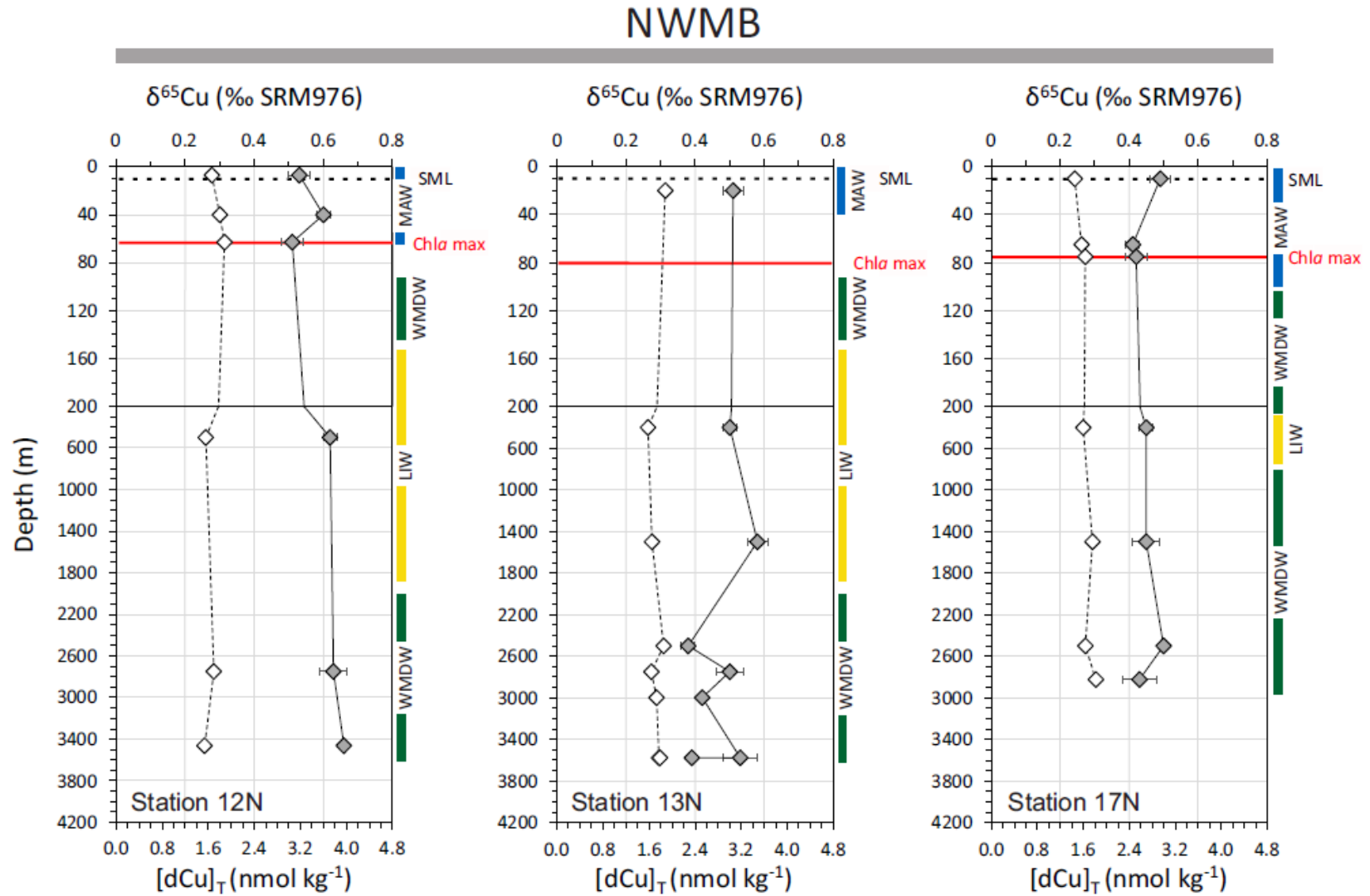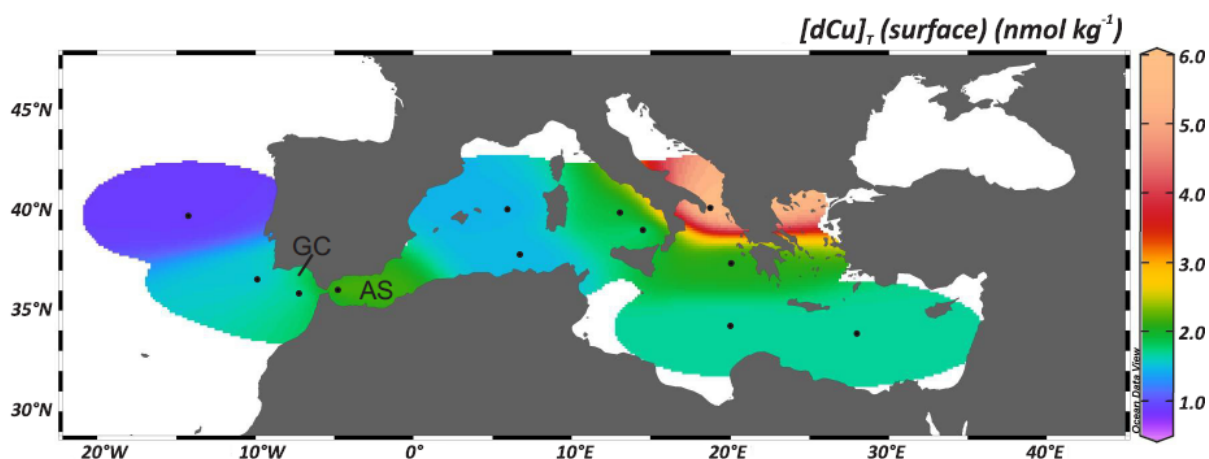
2

Figure 7: Isosurface variation of $[dCu]_T$ at ~10 m. Abbreviations shown in the map stand for: AS = Alboran Sea; GC = Gulf of Cadiz. Apart for station 5S in the Alboran Sea (case discussed in section 5.2.1), the Mediterranean stations show a South-West to North-East increase in concentration.

Tables and Table captions

Table 1: Procedure for dissolved Cu isotope analysis in a seawater sample.

Pre-treatment of the seawater samples:		
Filtration: 0.2 μm		
Acidification: HCl to pH ~1.7		
Addition of H_2O_2: 0.03 wt%		
Chromatographic separation of Cu:		
(1) NTA resin (1 mL, wet volume)	*peristaltic pump ON*	
	conditioning	25 mL of 0.02M HCl
	sample loading	0.5L to 1L pre-weighed
	elution of major and trace elements	20 mL of 0.02M HCl
	peristaltic pump OFF	
	elution of Cu	10 mL of 1.4M HNO_3 (*)
	column cleaning	10mL 1.4M HNO_3
		3mL 18.2 MΩ water
(2) AG MP-1M (1 ml, wet volume)	conditioning	2 mL of 10M HCl
	sample loading	0.5 mL of 10M HCl
	elution of major and trace elements	3.5 mL of 10m HCl
	elution of Cu	12 mL of 5M HCl
	column cleaning	10 mL 3M HNO_3
		10 mL 18.2 MΩ water
		10 mL 1.2M HCl
(3) Sample evaporated on hot-plate and re-dissolved in concentrated HNO_3 (Optima™-Grade)		
(4) Sample evaporated and re-dissolved in 0.28M HNO_3 for MC ICP-MS analysis		
(*) Measurement of dissolved Cu concentration:		
0.4 mL of sample into 2 mL of 18.2 MΩ water for MC ICP-MS analysis		

Table 2: $[dCu]_T$ (nmol kg^{-1}) and $\delta^{65}Cu$ (‰) for the Geotraces inter-comparison exercise, using BATS seawater sampled in 2008. The consensus values for the North Atlantic reference samples are available at es.ucsc.edu (concentrations only). The errors reported on these values were adapted to be at 2s.d. When no duplicate was done, the concentration $[dCu]_T$ is reported at 5% RSD (96% confidence).

Station	#ID/Depth (m)	[dCu]$_T$ (nmol kg^{-1})	*2s.d.* *(nmol kg^{-1})*	N	δ^{65}Cu (‰)	*2s.d.* *(‰)*	N
Consensus values (2011): no UV before pre-concentration							
BATS	GS	0.83	*0.16*				
BATS	GD	1.55	*0.26*				
Boyle et al. (2012) : no UV before pre-concentration							
BATS	GS	0.74 - 0.89			0.56 - 0.63	*0.09*	
BATS	GD	1.16 - 1.22			0.56 - 0.57	*0.09*	
Takano et al. (2014) : no UV before pre-concentration							
BATS	GD				0.41	*0.05*	
Consensus values (2013) : use of UV before pre-concentration							
BATS	GS	0.84	*0.12*				
BATS	GD	1.62	*0.14*				
This study : no UV before pre-concentration							
BATS	GSI-72	0.81	*0.06*	2	0.42	*0.06*	3
BATS	GDI-74	1.38	*0.13*	2	0.62	*0.06*	3
1 (Atlantic)	23	0.89	*0.16*	3	0.41	*0.06*	9
1 (Atlantic)	1500	1.38		1	0.60	*0.08*	5

1

2

1 Table 3: Total dissolved Cu concentration ([dCu]$_T$) and δ^{65}Cu for the Atlantic stations, the
2 southern and northern Mediterranean Sea stations, along with absolute salinity (S$_A$),
3 conservative temperature (CT), density anomaly (σ$_θ$), chlorophyll a concentration (Chl a) and
4 dissolved oxygen concentration modified from ship-board data. When no duplicate was done,
5 the concentration [dCu]$_T$ is reported at 5% RSD at 96% confidence level.

Depth (m)	S$_A$ (g kg^{-1})	CT (°C)	σ$_θ$ (kg m^{-3})	Oxygen (µmol kg^{-1})	Chl a (mg m^{-3})	[dCu]$_T$ (nmol kg^{-1})	2s.d. (nmol kg^{-1})	N	δ^{65}Cu (‰)	2s.d. (‰)	N
Station 1 (39.733 °N - 14.167 °W; 5265 m)											
23	36.18	15.0	26.75	254.0	0.80	0.89	*0.16*	3	0.41	*0.06*	9
1499	35.80	7.4	27.85	214.0	0.00	1.38		1	0.60	*0.08*	5
Station 3 (36.566 °N - 9.866 °W; 3940 m)											
8	36.67	17.7	26.49	238.3	0.05	1.52	*0.00*	2	0.43	*0.06*	3
50	36.67	17.7	26.49	238.0	0.04	0.76		1	0.49	*0.06*	3
75	36.65	17.4	26.54	240.5	0.07	0.72		1	0.55	*0.06*	3
100	36.53	16.4	26.69	232.1	0.25	0.67		1	0.64	*0.06*	3
151	36.37	15.3	26.81	214.9	0.02	0.86		1	0.47	*0.06*	3
503	35.80	11.5	27.17	191.2	0.00	0.93		1	0.49	*0.06*	2
752	35.97	10.7	27.46	174.7	0.02	1.00		1	0.59	*0.06*	3
1001	36.11	10.1	27.67	177.8	0.00	1.01		1	0.55	*0.10*	3
2000	35.35	4.4	27.88	236.3	0.00	1.28		1	0.60	*0.06*	3
3251	35.10	2.4	27.88	240.5	0.00	1.93		1	0.60	*0.06*	3
3875	35.07	2.1	27.89	236.7	0.00	2.38		1	0.58	*0.06*	3
Station 4 (35.842 °N - 7.256 °W; 1053 m)											
10	36.62	18.0	26.38	234.8	0.05	1.56		1	0.30	*0.06*	4
59	36.59	16.5	26.71	244.1	0.44	0.80		1	0.50	*0.08*	3
68	36.59	16.3	26.76	234.8	0.22	0.77		1	0.47	*0.06*	3
100	36.58	16.1	26.81	226.6	0.05	0.93		1	0.43	*0.08*	3
144	36.53	15.7	26.84	222.7	0.01	0.81		1	0.54	*0.06*	2
174	36.49	15.6	26.86	222.1	0.01	0.76		1	0.43	*0.06*	2
398	35.99	12.9	27.03	202.8	0.00	0.84		1	0.33	*0.06*	3
801	35.89	10.3	27.46	167.1	0.00	0.89		1	0.54	*0.06*	2
1043	37.00	12.2	27.97	178.0	0.00	1.04		1	0.57	*0.06*	3
Station 5S (36.058 °N - 4.814 °W; 943 m)											
9	36.44	17.0	26.49	244.0	0.11	2.32	*0.04*	2	0.61	*0.06*	4
27	36.46	16.9	26.53	243.7	0.34	1.84		1	0.68	*0.08*	4
39	36.51	16.8	26.58	236.7	0.37	1.75		1	0.60	*0.08*	4
54	36.56	16.6	26.65	232.9	0.38	1.49		1	0.54	*0.07*	4
69	36.81	15.9	27.01	229.0	0.21	1.65	*0.11*	2	0.43	*0.18*	3
98	37.54	14.5	27.90	214.0	0.02	1.39		1	0.43	*0.06*	3
176	38.58	13.1	28.99	165.3	0.02	1.41		1	0.46	*0.06*	4
249	38.68	13.1	29.07	162.0	0.00	1.51	*0.02*	2	0.47	*0.16*	4
299	38.70	13.1	29.08	163.2	0.01	1.38		1	0.35	*0.06*	4
400	38.70	13.0	29.09	173.5	0.02	1.53	*0.03*	2	0.53	*0.06*	3
800	38.67	12.9	29.10		0.00	1.35		1	0.51	*0.06*	3
934	38.66	12.8	29.11		0.00	1.27		1	0.53	*0.07*	4

6

Depth	SA	CT	σ_θ	Oxygen	Chl a	[dCu]$_T$	2s.d.	N	δ^{65}Cu	2s.d.	N
(m)	(g kg^{-1})	(°C)	(kg m^{-3})	(μmol kg^{-1})	(mg m^{-3})	(nmol kg^{-1})	(nmol kg^{-1})		(‰)	(‰)	
Station 11S (37.778 °N - 6.663 °E; 2871 m)											
10	37.28	17.4	27.03	222.8	0.10	1.47	0.18	2	0.42	0.06	5
40	37.28	15.1	27.65	231.3	0.30	4.30	0.12	2	0.23	0.06	3
53	37.44	14.7	27.78	226.7	0.62	2.47	0.06	2	0.39	0.06	3
71	37.64	14.5	27.97	216.3	0.07				0.48	0.06	2
100	37.99	14.0	28.35	207.3	0.02	1.47		1	0.46	0.06	4
303	38.74	13.4	29.05	157.3	0.00	1.32		1	0.49	0.06	1
400	38.77	13.3	29.08	160.7	0.01	1.48		1	0.48	0.06	3
751	38.74	13.1	29.10	165.9	0.01	1.43		1	0.51	0.06	3
1252	38.66	12.8	29.11	174.7	0.00	1.58		1	0.41	0.06	3
2250	38.66	12.8	29.11	182.0	0.01	1.52		1	0.52	0.06	4
2830	38.67	12.8	29.12	183.7	0.01	3.04	0.20	2	0.45	0.06	3
Station 18S (34.284 °N - 20.016 °E; 3263 m)											
9	39.22	20.5	27.67	231.9	0.02	1.66	0.09	2	0.61	0.19	6
41	39.22	17.5	28.47	255.0	0.04	2.01	0.01	2	0.49	0.07	3
60	39.20	16.3	28.74	250.7	0.05	2.14	0.01	2	0.51	0.06	3
101	39.20	15.4	28.94	223.5	0.10	1.66		1	0.59	0.06	2
125	39.19	15.2	28.99	212.8	0.09	1.99		1	0.37	0.06	2
300	39.12	14.4	29.13	197.7	0.00	1.61		1	0.47	0.13	2
600	39.02	13.9	29.16	191.3	0.02	1.62	0.05	2	0.66	0.06	3
1499	38.93	13.4	29.19	198.9	0.00	2.27	0.15	2	0.34	0.06	3
2750	38.91	13.3	29.20	205.2	0.01	2.61	0.79	2	0.66	0.06	3
3263	39.02	13.3	29.28	200.8	0.02	2.05	0.12	2	0.49	0.06	2
Station 21S (33.843 °N - 28.082 °E; 2673 m)											
10	38.97	21.6	27.18	227.8	0.04	1.68	0.15	2	0.21	0.06	5
40	38.85	17.5	28.19	250.2	0.04	1.37	0.01	2	0.62	0.06	3
85	39.06	16.4	28.61	236.5	0.09	4.22	0.13	2	0.67	0.06	3
101	39.17	16.5	28.68	236.0	0.06	1.89	0.03	2	0.60	0.06	4
115	39.18	16.2	28.76	232.8	0.05	1.72		1	0.53	0.11	2
301	39.18	14.7	29.11	212.3	0.00	1.17	0.04	2	0.68	0.06	3
501	39.02	13.9	29.16	189.7	0.02	1.62	0.33	2	0.54	0.06	3
1500	38.94	13.5	29.18	193.1	0.01	1.62	0.01	2	0.76	0.06	3
2380	38.96	13.5	29.20	198.5	0.02	1.52		1	0.66	0.06	3
Station 5N (37.378 °N - 20.164 °E; 3875 m)											
10	39.32	25.5	26.25	203.0	0.03	2.05		1	0.40	0.06	3
50	39.00	16.6	28.53	267.3	0.06	2.24		1	0.47	0.06	3
80	39.04	15.2	28.89	233.3	0.26	2.01		1	0.41	0.07	3
1000	38.96	13.6	29.18	179.1	0.02	1.71		1	0.67	0.19	4
2000	38.93	13.4	29.19	186.0	0.02	1.91		1	0.67	0.06	3
3250	38.91	13.3	29.20	188.2	0.01	1.95		1	0.45	0.06	2
3812	38.92	13.3	29.20	187.5	0.01	2.59		1	0.62	0.06	3

1

2

Depth	SA	CT	σ_θ	Oxygen	Chl a	$[dCu]_T$	2s.d.	N	$\delta^{65}Cu$	2s.d.	N
(m)	(g kg^{-1})	(°C)	(kg m^{-3})	(µmol kg^{-1})	(mg m-3)	(nmol kg^{-1})	(nmol kg^{-1})		(‰)	(‰)	
Station 9N (40.154 °N - 18.817 °E; 739 m)											
10	38.81	24.9	26.06	208.8	0.03	6.00	0.19	2	0.51	0.06	3
25	39.08	17.0	28.47	248.5	0.04	2.20		1	0.44	0.11	4
58	39.04	15.1	28.91	236.3	0.28	1.95	0.06	2	0.58	0.06	3
145	39.13	14.8	29.03	209.4	0.02	1.91	0.14	2	0.59	0.07	3
205	39.14	14.7	29.06	206.3	0.02	1.96		1	0.55	0.06	2
340	39.07	14.2	29.11	206.5	0.02	1.99		1	0.58	0.06	3
739	38.94	13.4	29.21	213.9	0.02	2.32		1	0.54	0.11	3
Station 12N (39.007 °N - 14.502 °E; 3464 m)											
7	38.18	26.0	25.26	195.4	0.04	1.66	0.10	2	0.53	0.02	4
40	37.98	15.6	27.97	255.1	0.06	1.80	0.16	2	0.60	0.12	5
63	38.23	14.4	28.45	227.1	0.28	1.88	0.24	2	0.51	0.06	5
500	38.95	14.0	29.08	176.9	0.02	1.56	0.08	2	0.62	0.15	4
2749	38.69	12.9	29.11	178.7	0.02	1.70	0.18	2	0.63	0.11	5
3464	38.68	12.9	29.11	176.3	0.01	1.54	0.00	2	0.66	0.09	6
Station 13N (39.878 °N - 13.010 °E; 3576 m)											
20	38.07	20.9	26.71	249.2	0.04	1.88		1	0.51	0.06	3
400	38.95	14.0	29.07	175.7	0.02	1.58		1	0.50	0.07	3
1500	38.74	13.1	29.11	178.4	0.02	1.65		1	0.58	0.06	3
2500	38.69	12.9	29.11	179.4	0.02	1.85		1	0.38	0.06	2
2750	38.69	12.9	29.11	180.4	0.02	1.64		1	0.50	0.06	3
2999	38.68	12.9	29.11	181.0	0.01	1.73		1	0.42	0.06	3
3576	38.68	12.9	29.11	181.0	0.01	1.77		1	0.53	0.06	3
3576	38.68	12.9	29.11	181.0	0.02	1.79	0.10	2	0.39	0.06	3
Station 17N (40.069 °N - 5.947 °E; 2824 m)											
10	37.89	26.6	24.87	206.4	0.04	1.45	0.11	2	0.49	0.06	2
65	37.71	15.6	27.76	253.7	0.24	1.57	0.06	2	0.41	0.06	2
75	37.80	15.0	27.97	237.0	0.67	1.63	0.02	2	0.42	0.06	3
400	38.75	13.3	29.09	175.7	0.02	1.60		1	0.45	0.06	2
1500	38.66	12.8	29.11	190.3	0.02	1.76	0.04	2	0.45	0.06	3
2499	38.67	12.8	29.12	194.0	0.02	1.64		1	0.50	0.06	3
2824	38.68	12.8	29.12	195.3	0.02	1.82		1	0.43	0.06	3

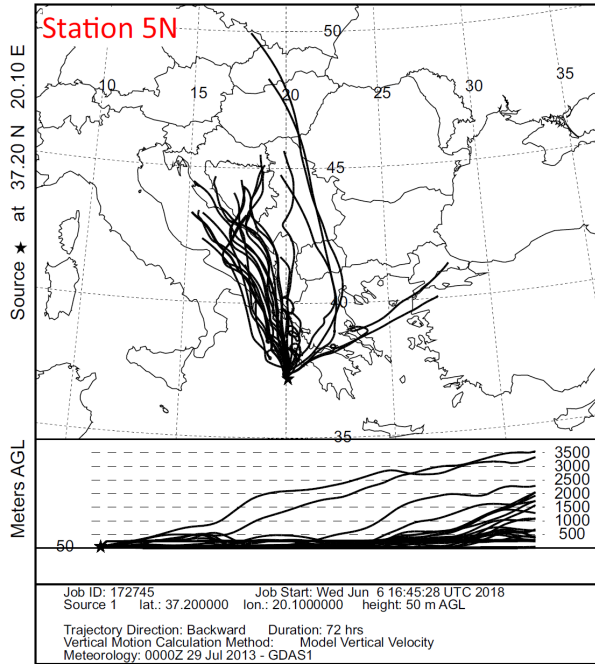1 **Supplementary material captions (see separate file)**

2 Supplementary figure 1: Air flow backtrajectory modelized for all Mediterranean Sea stations.
3 Figures are plotted using NOAA's HYSPLIT backtrajectory model provided by Air Resources
4 Laboratory of NOAA, tracking back air flow for 72 hours at 50 m of altitude (Rolph et al.,
5 2015; Stein et al., 2015).

6 Supplementary equation 1: Modified mixing equation between a sedimentary source and the
7 overlying deep water.

1   Supplementary table 1: Calculated $\delta^{65}Cu$ of the sediment source ($\delta^{65}Cu_{(sed)}$; ‰) for Atlantic
2   and Mediterranean Sea stations which showed increase of $[dCu]_T$ at benthic depth. See
3   supplementary equation 1 for further details on the parameters.
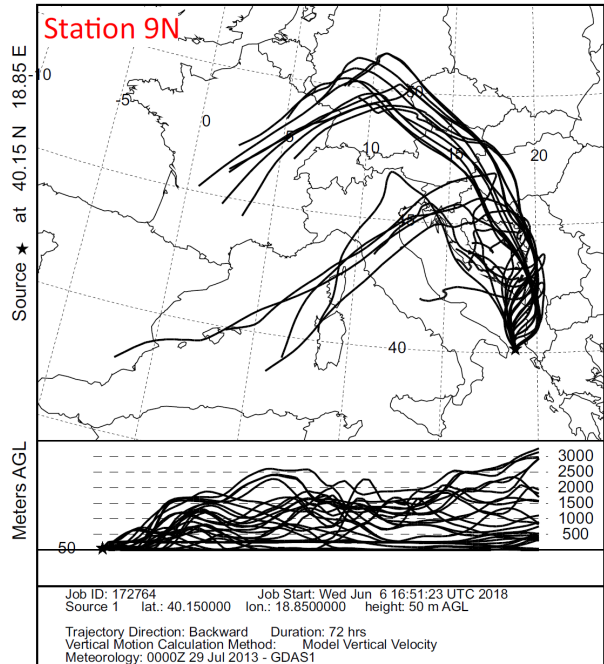
Supplementary figure 1: Air flow backtrajectory modelized for all Mediterranean Sea stations. Figures are plotted using NOAA's HYSPLIT backtrajectory model provided by Air Resources Laboratory of NOAA, tracking back air flow for 72 hours at 50 m of altitude (Rolph et al., 2015; Stein et al., 2015).
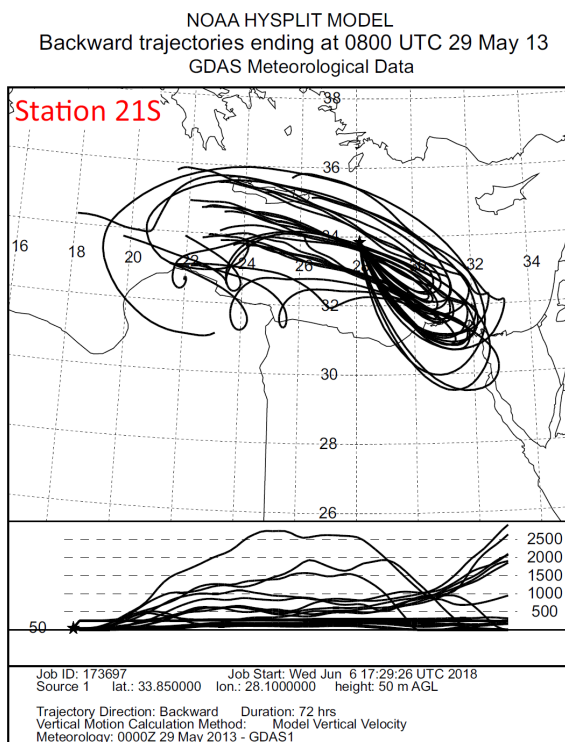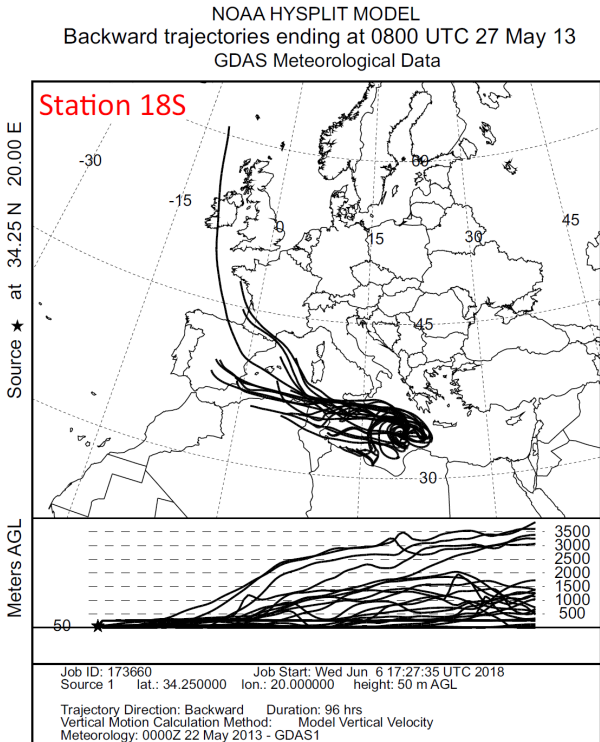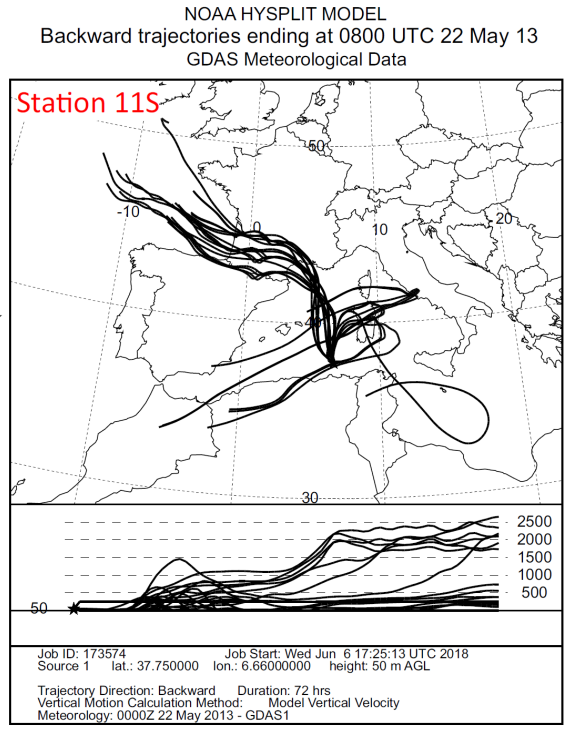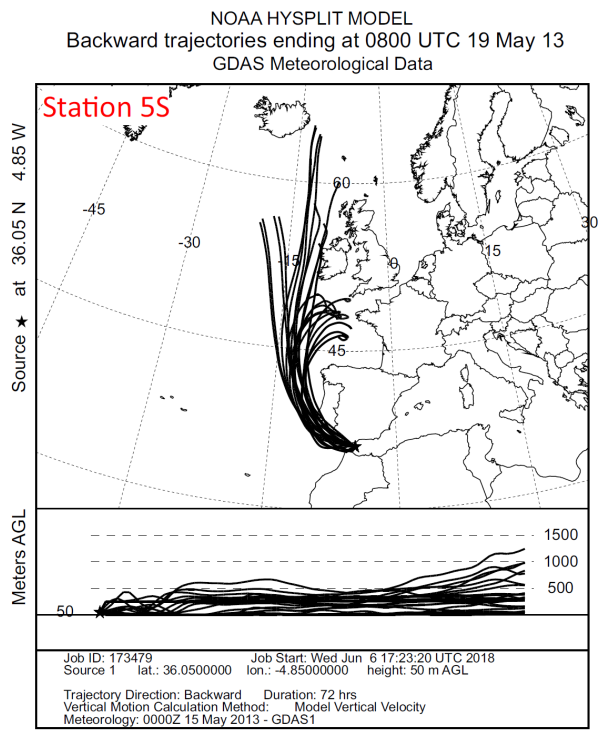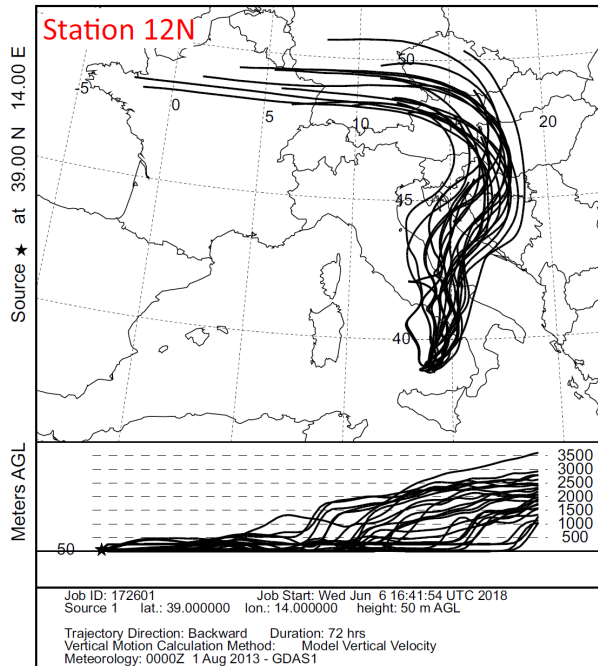
NOAA HYSPLIT MODEL
Backward trajectories ending at 1200 UTC 29 Jul 13
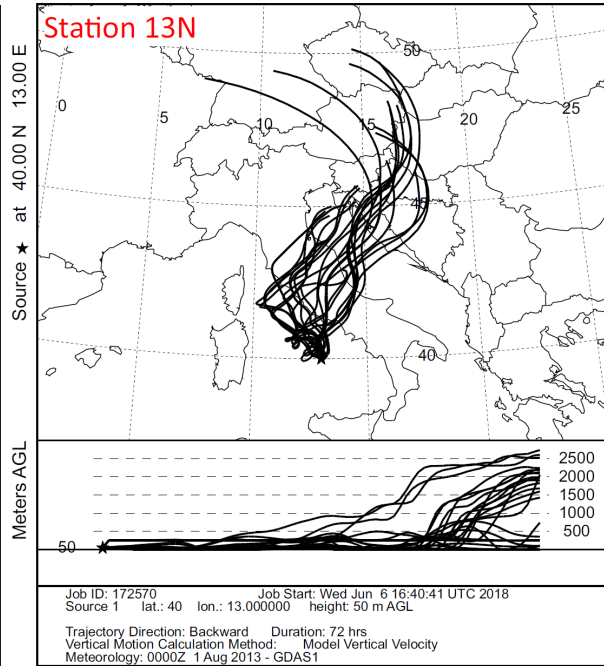GDAS Meteorological Data

Station 5N

Job ID: 172745   Job Start: Wed Jun 6 16:45:28 UTC 2018
Source 1   lat.: 37.200000   lon.: 20.1000000   height: 50 m AGL

Trajectory Direction: Backward   Duration: 72 hrs
Vertical Motion Calculation Method: Model Vertical Velocity
Meteorology: 0000Z 29 Jul 2013 - GDAS1

NOAA HYSPLIT MODEL
Backward trajectories ending at 1200 UTC 31 Jul 13
GDAS Meteorological Data

Station 9N

Job ID: 172764   Job Start: Wed Jun 6 16:51:23 UTC 2018
Source 1   lat.: 40.150000   lon.: 18.8500000   height: 50 m AGL

Trajectory Direction: Backward   Duration: 72 hrs
Vertical Motion Calculation Method: Model Vertical Velocity
Meteorology: 0000Z 29 Jul 2013 - GDAS1

NOAA HYSPLIT MODEL
Backward trajectories ending at 1600 UTC 02 Aug 13
GDAS Meteorological Data

Station 12N

Job ID: 172601   Job Start: Wed Jun 6 16:41:54 UTC 2018
Source 1   lat.: 39.000000   lon.: 14.000000   height: 50 m AGL

Trajectory Direction: Backward   Duration: 72 hrs
Vertical Motion Calculation Method: Model Vertical Velocity
Meteorology: 0000Z 1 Aug 2013 - GDAS1

NOAA HYSPLIT MODEL
Backward trajectories ending at 0800 UTC 03 Aug 13
GDAS Meteorological Data

Station 13N

Job ID: 172570   Job Start: Wed Jun 6 16:40:41 UTC 2018
Source 1   lat.: 40   lon.: 13.000000   height: 50 m AGL

Trajectory Direction: Backward   Duration: 72 hrs
Vertical Motion Calculation Method: Model Vertical Velocity
Meteorology: 0000Z 1 Aug 2013 - GDAS1
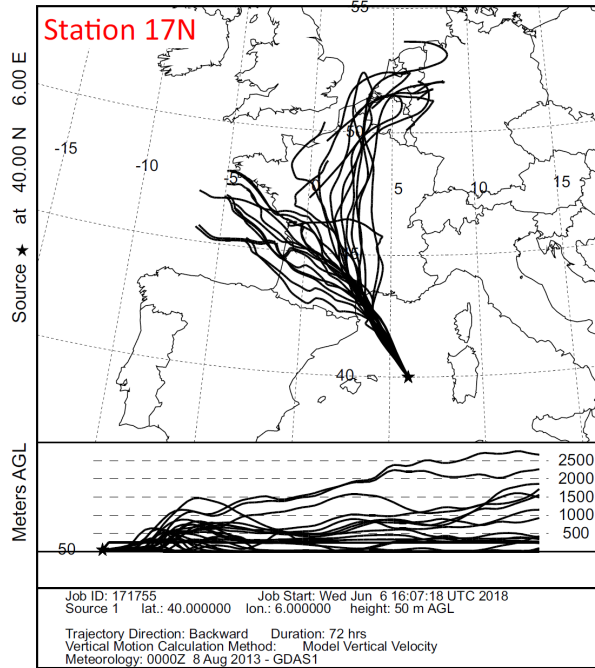
Supplementary equation 1: Modified mixing equation between a sedimentary source and the overlying deep water.

$$\delta^{65}Cu_{(sed)} = \frac{\delta^{65}Cu_{(mix)} - \delta^{65}Cu_{(SW)} \times (1 - X)}{X}$$

With $\delta^{65}Cu_{sed}$ being the isotope ratio of the dissolved Cu remobilized from the sediment, $\delta^{65}Cu_{mix}$ is the isotope ratio measured at bottom depth, $\delta^{65}Cu_{SW}$ is the isotope ratio measured in the deep-water mass above bottom depth, and X is the mass fraction of dCu added to the bottom from the sediment, and is defined as $X = 1 - [dCu]_{T(SW)}/ [dCu]_{T(mix)}$. We did not do an average of $\delta^{65}Cu_{SW}$ on the deep water column (200 m – bottom) to better take into account the benthic variation in dCu isotope composition observed.

Supplementary table 1: Calculated $\delta^{65}Cu$ of the sediment source ($\delta^{65}Cu_{(sed)}$; ‰) for Atlantic and Mediterranean Sea stations which showed increase of $[dCu]_T$ at benthic depth. See supplementary equation 1 for further details on the parameters.

Station #	3	11S	9N	17N
$[dCu]_{T(SW)}$ (nmol kg^{-1})	1.93	1.52	1.99	1.64
$[dCu]_{T(mix)}$ (nmol kg^{-1})	2.38	3.04	2.32	1.82
$\delta^{65}Cu_{(SW)}$ (‰ SRM976)	0.6	0.52	0.58	0.5
$\delta^{65}Cu_{(mix)}$ (‰ SRM976)	0.58	0.45	0.54	0.43
X	0.19	0.50	0.14	0.10
$\delta^{65}Cu_{(sed)}$ (‰)	0.49	0.38	0.30	-0.21

Supplementary references :

Rolph, G., Stein, A. and Stunder, B., 2015. Real-time Environmental Applications and Display sYstem: READY. Environmental Modelling & Software, 95: 210-228.

Stein, A.F. et al., 2015. NOAA's HYSPLIT atmospheric transport and dispersion modeling system. Bulletin of American Meteorological Society, 96: 2059-2077.